Physics of Living Systems

Cyclic muscle contractions reinforce the acto-myosin motors and mediate the full elongation of *C. elegans* embryo

Anna Dai, Martine Ben Amar

Laboratoire de Physique de l'Ecole normale supérieure, ENS, Université PSL, CNRS, Sorbonne Université, Université Paris Cité, F-75005 Paris, France

Reviewed Preprint

Revised by authors after peer review.

About eLife's process

Reviewed preprint version 2
April 10, 2024 (this version)

Reviewed preprint version 1
November 10, 2023

Posted to preprint server
August 15, 2023

Sent for peer review
August 1, 2023

Abstract

The paramount importance of mechanical forces in morphogenesis and embryogenesis is widely recognized, but understanding the mechanism at the cellular and molecular level remains challenging. Because of its simple internal organization, Caenorhabditis elegans is a rewarding system of study. As demonstrated experimentally, after an initial period of steady elongation driven by the actomyosin network, muscle contractions operate a quasi-periodic sequence of bending, rotation and torsion, that leads to the final 4-fold size of the embryo before hatching. How actomyosin and muscles contribute to embryonic elongation is investigated here theoretically. A filamentary elastic model that converts stimuli generated by biochemical signals in the tissue into driving forces, explains embryonic deformation under actin bundles and muscle activity, and dictates mechanisms of late elongation based on the effects of energy conversion and dissipation. We quantify this dynamic transformation by stretches applied to a cylindrical structure that mimics the body shape in finite elasticity, obtaining good agreement and understanding for both wild-type and mutant embryos at all stages.

eLife assessment

Using continuum theory of elastic solids the authors present evidence that periodic muscle contraction leads to elongation of C. elegans embryos by storing elastic energy that is subsequently released by extending the embryo's long axis. This **important** finding could apply to other developmental processes and be exploited in soft robotics. The presented evidence is **convincing** on the phenomenological level adopted in the work. How bending energy is converted into elongation on a more microscopic level remains to be worked out.

Introduction

Mechanical stresses play a critical role during embryogenesis, affecting complex biological tissues such as the skin, the brain, and the interior of organs. There are many studies in recent decades, for example, the pattern of the intestine (Coulombre and Coulombre (1958); Hannezo et al. (2011); Li et al. (2011); Ben Amar and Jia (2013); Shyer et al. (2013)), the brain cortex (Toro and Burnod (2005); Goriely et al. (2015); Ben Amar and Bordner (2017); Tallinen et al. (2016)), and the circumvolutions of the fingerprints (Kücken and Newell (2005); Ciarletta and Ben Amar (2012)), which have been interpreted as the result of compressive stresses generated by the growth that occurs a few months after fertilization in humans. The superposition of mechanical stresses, cellular processes (e.g., division, migration), and tissue organization is often too complex to identify and quantify. For example, independent of growth, stresses can be generated by different molecular motors, among which myosin II, linked to actin filaments, is the most abundant during epithelial cell morphogenesis (Vicente-Manzanares et al. (2009)) and cell motility (Cowan and Hyman (2007); Olson and Sahai (2009); Palumbo et al. (2022)). Spatial distribution and dynamics of myosin II strongly influence the morphogenetic process (Levayer and Lecuit (2012); Lv et al. (2022)), as demonstrated for Drosophila (Bertet et al. (2004); Blankenship et al. (2006); Saxena et al. (2014); Shindo and Wallingford (2014)) and also for *C. elegans* embryos (Priess and Hirsh (1986); Gally et al. (2009); Ben Amar et al. (2018)).

Embryonic elongation of C. elegans before hatching provides an attractive model of matter reorganization in the absence of growth. It occurs after ventral enclosure and takes about 240 minutes to transform the lima bean-shaped embryo into the final elongated worm form: the embryo elongates four times along the anterior/posterior axis by (McKeown et al. (1998)). The short lifespan of the egg before hatching and its transparency make this system ideal for studying the forces that exist at or near the cortical epithelium. However, in contrast to Drosophila and zebrafish embryonic development, there is no cell migration, cell division, or significant change in embryonic volume (Sulston et al. (1983); Priess and Hirsh (1986)), only remarkable epidermal elongation drives the entire morphogenetic process of *C. elegans* in the post-enclosure period. There are two experimentally identified driving forces for the elongation: the actomyosin contractility in the seam cells of the epidermis, which appears to persist throughout the whole elongation process, and the muscle activity beneath the epidermis, which begins after the 1.7 ~ 1.8-fold stage. The transition is well defined, because the muscle involvement makes the embryo rather motile, and any physical experiments such as laser fracture ablation of the epidermis, which could be performed and achieved in the first period (***Vuong-Brender et al. (2017a)***), become difficult. Consequently, the elongation process of *C. elegans* could be divided into two stages: the early elongation and the late elongation, depending on the muscle activation, and **Fig.1(A)** shows the whole elongation process (***Vuong-Brender et al. (2017a)***). Previously, the role of the actomyosin network in the seam cells during the *C. elegans* early elongation was investigated (Ben Amar et al. (2018)). Based on the geometry of a hollow cylinder composed of dorsal, ventral and seam cells, a model including the pre-stress responsible for the enclosure, the active compressive ortho-radial stress combined with the passive stress quantitatively predicts the elongation, but only up to ~ 70% of the initial length.

For the late elongation phase, the actomyosin network and the muscles together drive the full elongation during this phase (***Vuong-Brender et al. (2017a)***). The muscles play an important role and mutants with muscle defects are unable to complete the elongation process, even though the actomyosin network functions normally (Lardennois et al. (2019)). **Fig.1(B)** shows a schematic image of the *C. elegans* body (Zhang et al. (2011)) with four rows of muscles, two of which are under the dorsal epidermis and the other two are under the ventral epidermis. As observed *in vivo, C. elegans* exhibits systematic rotations accompanying each contraction (Yang (2017); Yang Xinyi et al. (2023)), and deformations such as bending and twisting. Eventually, the *C. elegans*

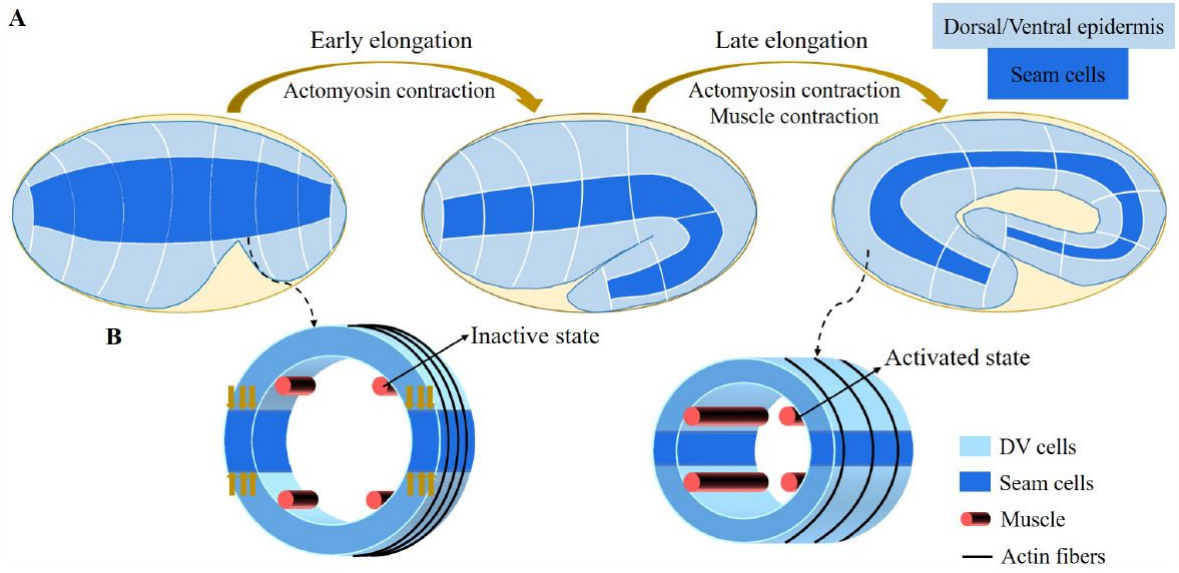

Figure 1.

(A) Overview of *C. elegans* embryonic development. Three epidermal cell types are found around the circumference: dorsal, ventral and seam cells. (B) Schemes showing a *C. elegans* crossn section of the embryo. Small yellow arrows in the left image indicate the contraction force that occurred in the seam cell. Four muscle bands under the epidermis and actin bundles surround the outer epidermis.

embryo will undergo an elongation of 1.8-fold to 4-fold. As the activated muscle contracts on one side, the contractile forces are transmitted to the epidermis on that side. Since striated muscles can only perform cycles of contraction and relaxation, their action will tend to reduce the length of the embryo. Therefore, it is necessary to understand how the embryo elongates during each contraction and how the muscle contractions are coupled to the actomyosin activity. This work aims to answer this paradox within the framework of finite elasticity without invoking cellular plasticity and stochasticity, which cannot be considered as driving forces. In addition, several important questions remain unanswered at the late stage of elongation. First of all, we may also observe a torsion of the embryo, but if the muscle activity suggests a bending, this alone cannot explain alone a substantial torsion. Second, a small deviation of the muscle axis (Moerman and Williams (2006)) is responsible for a number of rotations, how to relate these rotations to the muscle activation (Yang (2017)). Since any measurement on a motile embryo at this scale is difficult, it is useful to explore the mechanism of late elongation theoretically. Furthermore, muscle contraction is crucial for both biological development and activities and has been extensively studied by researchers (Tan and De Vita (2015); De Vita et al. (2017)), but how it works at small scales remains to be understood.

Using a finite elasticity model and assuming that the embryonic body shape is cylindrical, we can evaluate the geometric bending deformation and the energy released during each muscle contraction on one side since after each contraction, the muscles relax and then the muscles on the opposite side undergo a new contraction. This cyclic process results in a tiny elongation of the cylinder along its axis of symmetry with each contraction. Each of these contractions correlates with the rotational movements of the embryo (Yang (2017)). By repeating these pairs of contractions more than two hundred times, a cumulative extension is achieved, but it must be reduced by friction mechanisms, also evaluated by the model. Furthermore, the mechanical model explains the existence of a torque acting on the position of the head or tail by the coupling of the muscle contraction with the orthoradial actomyosin forces. Finally, the small deviation between the muscles and the central axis experimentally detected (Moerman and Williams (2006)) induces cyclic rotations and possibly torsions leading to fluid viscous flow inside the egg. The quantification of all these processes allows the evaluation of physical quantities of the embryo, such as the shear modulus of each component, the interstitial fluid viscosity and the active forces exerted by the actomyosin network and the muscles, which are poorly y known in the embryonic stages.

Our mechanical model accounts for the dynamic deformations induced by the internal stimuli of a layered soft cylinder, allowing us to make accurate quantitative predictions about the active networks of the embryo. Furthermore, our model accounts for the dissipation that occurs in the late period just before the embryo hatches. Our results are consistent with observations of actomyosin and muscle activity (***Vuong-Brender et al. (2017a)***; Ben Amar et al. (2018); Lardennois et al. (2019)). The architecture of our work is illustrated in **Fig.2**.

Results

It is widely recognized that *C. elegans* is a well-established model organism in the field of developmental biology. However, it is less well known that its internal striated muscles share similarities with vertebrate skeletal muscles in terms of both function and structure (Lesanpezeshki et al. (2021)). Since they are contractile, the role of the four axial muscles (as shown in **Fig.1**) in the final shaping of the embryo is almost counterintuitive. In this section, we aim to elucidate the action of these muscles when coupled to the actomyosin network, using a purely mechanical approach. To achieve a quantitative understanding, our method requires a detailed description of the deformation geometry of the embryo, where the body shape is represented by a fully heterogeneous cylinder.

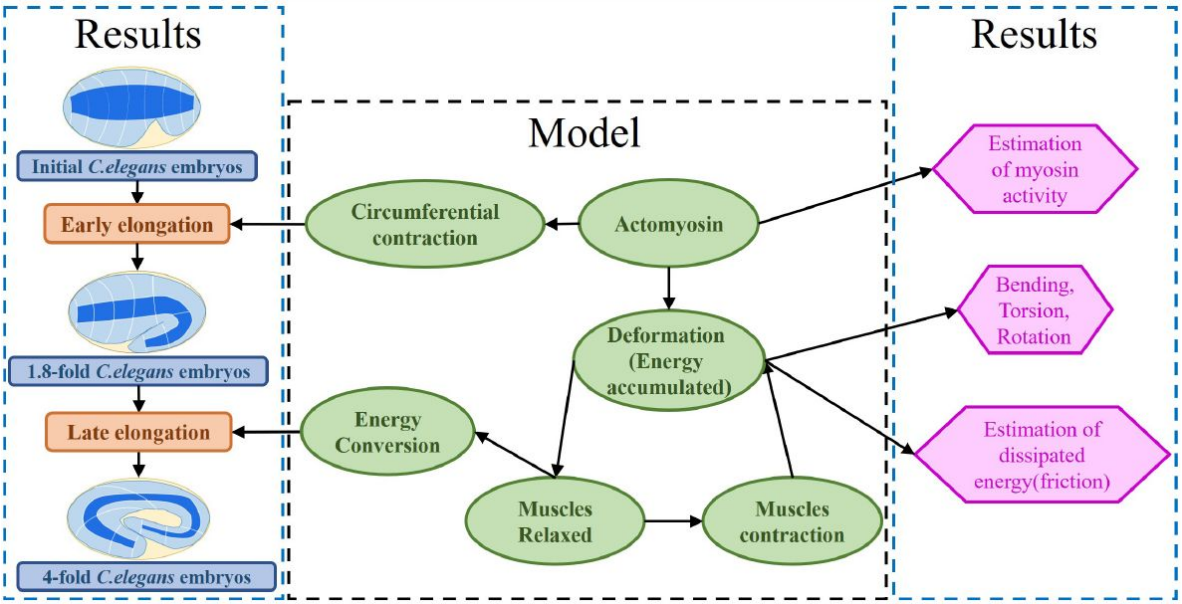

Figure 2.

Architecture of the program. The program reflects the framework of the research. On the one hand, the proposed model explains the early and late elongation of the *C. elegans*, on the other hand, the early myosin activity is estimated, the deformations (bending, twisting, rotation) occurring in the late period are recovered, and the estimation of the energy dissipated during muscle activity is achieved.

Geometric and strain deformations of the embryo

The early elongation of the *C. elegans* embryo has been previously studied, which is characterized by an inner cylinder surrounded by epithelial cells located in the cortical position (Ben Amar et al. (2018)). The cortex is composed of three distinct cell types - the seam, dorsal, and ventral cells - that exhibit a unique cytoskeletal organization and actin network configuration. Among these, only the seam cells possess active myosin motors that function in the ortho-radial direction, allowing for the circumferential contraction and thereby triggering the early elongation process. In this study, we simplify the cylindrical geometry of the body and treat the epidermis as a unified whole with effective activity localized along the circumference, supported by four muscles distributed beneath the epidermis. The muscles do not play a role in the early elongation phase and have therefore not been considered previously (***Vuong-Brender et al. (2017a)***; Ben Amar et al. (2018)). After this period of approximately a 1.8-fold increase in length, muscles parallel to the main axis and actin bundles organized along the circumference will cooperate to drive further elongation. **Table. 1** provides the size parameters of *C. elegans* that will be used hereafter.

We focus on the total deformation of a full cylinder or a thin rod with a length L greater than the radius R and a central vertical axis along the Z direction. Contrary to previous works (Ciarletta et al. (2009); Ben Amar et al. (2018)), here we decide to simplify the geometrical aspect due to the mechanical complexity. The biological activity induced by the actomyosin network and muscles is represented by active strains, and the global shape is the result of the coupling between elastic and active strains, modulated by dissipation. Active strains are generated by non-mechanical processes (e.g., biochemical processes): myosin motors and striated muscles derive their energy from ATP hydrolysis, which is converted into mechanical fiber contractions. Due to the significant deformation observed, the central line is distorted and becomes a curve in three-dimensional space, represented by a vector $\mathbf{r}(\mathbf{Z})$, as depicted in **Fig.3(A)**. Along this curve, perpendicular planar sections of the embryo can be defined, and the deformation in each section can be quantified since the circular geometry is lost with the contractions (Kaczmarski et al. (2022)). The geometric mapping is as follows:

$$\chi(\mathbf{X}) = \mathbf{r}(Z) + \sum_{i=1}^{3} \varepsilon a_i(\varepsilon R, \Theta, Z)\,\mathbf{d}_i(Z), \tag{1}$$

where the a_i represents the deformation in each direction of the section with $a_i(0, \Theta, Z) = 0$ so that the Z-axis is mapped to the centerline $\mathbf{r}(Z)$. The small quantity ε is the ratio between the radius R and the length L of the cylinder. The axial extension ζ is given by $\mathbf{r}'(Z) = \zeta\,\mathbf{d}_3$, where' denotes the first derivative with respect to the material coordinate Z. From the director basis, the Darboux curvature vector reads: $\mathbf{u} = u_1\mathbf{d}_1 + u_2\mathbf{d}_2 + u_3\mathbf{d}_3$, this vector gives the evolution of the director basis along the filamentary line as: $\mathbf{d}_i'(Z) = \zeta\,\mathbf{u} \times \mathbf{d}_i$, see **Fig.3(A)**. Based on the model proposed by B. Kaczmarki *et al.* (Kaczmarski et al. (2022)), we define the initial configuration $\mathcal{B}_0$ with material points (R, Θ, Z), and the mapping function $\chi(\mathbf{X})$ connects the initial configuration $\mathcal{B}_0$ to the current configuration $\mathcal{B}$. The geometric deformation gradient is $\mathbf{F} = \mathrm{Grad}\chi = \mathbf{F_e G}$ (Nardinocchi and Teresi (2007)), where $\mathbf{G}$ is the active strain generated by the actomyosin or the muscles, and $\mathbf{F_e}$ is the elastic strain tensor.

Because of the two stages through which the *C. elegans* elongates, we need to evaluate the influence of the *C. elegans* actin network during the early elongation before studying the deformation at the late stage. Thus, the deformation gradient can be decomposed into: $\mathbf{F} = \mathbf{F}_e\mathbf{G}_1\mathbf{G}_0$ (Goriely and Ben Amar (2007)) where $\mathbf{G}_0$ refers to the pre-strain of the early period and $\mathbf{G}_1$ is the muscle supplementary active strain in the late period. Actin is distributed in a circular pattern in the outer epidermis, see **Fig.3(B)**, so the finite strain $\mathbf{G}_0$ is defined as $\mathbf{G}_0 = Diag(1, g_0(t), 1)$,

	Initial	1.8-fold
Radius	11.1 μm	8.2 μm
Length	50 μm	90 μm

Table 1.

Adopted real size parameters of the *C. elegans* (*Vuong-Brender et al. (2017a)*; *Ben Amar et al. (2018)*).

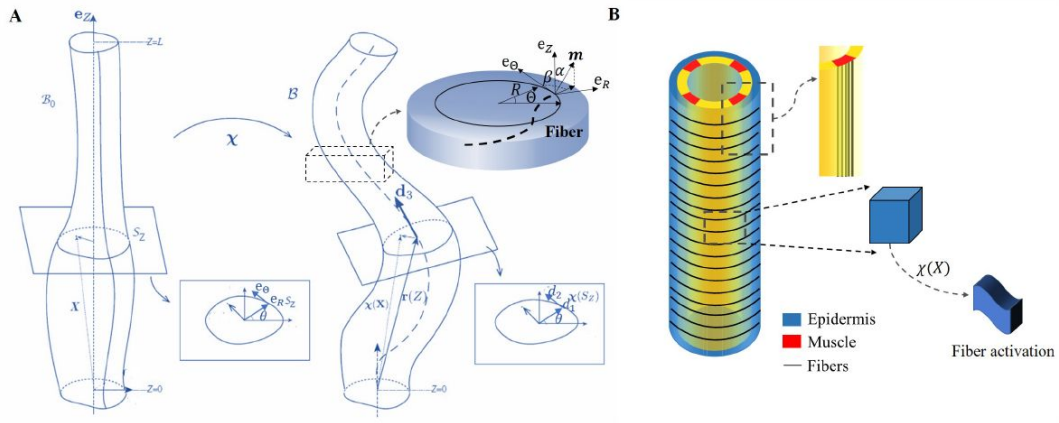

Figure 3.

(A) Cylindrical structure in the reference configuration (left) with a vertical centerline and its deformation in the current configuration (right). The deformed configuration is fully parameterized by the centerline **r** (*Z*) (resulting from the distortion of the central axis) and the deformation of each cross section. (B) Schematic representation of the body shape of the *C. elegans* embryo with the cortical epidermis and the four muscles. The fibers are embedded in the cortex. The blue part representing the epidermis shows the outer distribution of the actin organized in horizontal hoop bundles when the muscles are not activated. The yellow part includes the vertical red muscles, represented by axial fibers.

where $0 < g_0 < 1$ is the time-dependent decreasing eigenvalue, operating in the actin zone and is equal to unity in the other parts: $g_0(0) = 1$. In the case without pre-strain, $\mathbf{G}_0 = \mathbf{I}$. The deformation gradient follows the description of **Eq.(1)** :$\mathbf{F} = F_{ij}\mathbf{d}_i \otimes \mathbf{e}_j$, *where* $i \in \{1, 2, 3\}$ and $j \in \{R, \Theta, Z\}$.

Considering a filamentary structure **Fig.3(B)** with different fiber directions $\mathbf{m}$, these directions are specified by two angles α and β, as outlined in (Holzapfel (2000)): $\mathbf{m} = \sin\alpha \sin\beta\, \mathbf{e_R} + \sin\alpha \cos\beta\, \mathbf{e_\Theta} + \cos\alpha\, \mathbf{e_Z}$, $\alpha, \beta \in [-\pi/2, \pi/2]$. For muscle fibers, $\alpha_m = 0$ and $\beta_m = 0$, while for hoop fibers in the actin network, $\alpha_a = \pi/2$ and $\beta_a = 0$. When the muscles are activated and bend the embryo, the actin fibers are tilted with a tilt α, such that $-\pi/2 < \alpha_a < \pi/2$, $\alpha_a \neq 0$, and $\beta_a = 0$. Each active strain is represented by a tensor $\mathbf{G_i} = \mathbf{I} + \varepsilon \mathbf{g_i} \mathbf{m_i} \otimes \mathbf{m_i}$, where g_i represents the activity (g_m for muscles and g_a for actomyosin), and since both are contractile, their incremental activities are negative. Additional calculation details are provided in Section Methods and Materials.

To relate the deformations to the active forces induced by the muscles and the actomyosin network, we assume that the embryo can be represented by the simplest nonlinear hyperelastic model, called Neo-Hookean, with a strain energy density given by $W(\mathbf{F}_e) = \frac{\mu}{2}\left(tr\left(\mathbf{F}_e\mathbf{F}_e^T\right) - 3\right)$. In cylindrical coordinates, the total energy of the system and the associated energy density is:

$$\begin{aligned} \mathcal{W} &= \varepsilon^2 \int_0^L \mathrm{d}Z \int_S V(\mathbf{F}_e, \mathbf{G}) R \,\mathrm{dR}\,\mathrm{d}\Theta, \\ V &= W(\mathbf{F}_e) - p(J-1). \end{aligned} \tag{2}$$

where $J = \det \mathbf{F}_e$, p is a Lagrange multiplier that ensures the incompressibility of the sample, a physical property assumed in living matter. If the cylinder contains several layers with different shear modulus μ and different active strains, the integral over S covers each layer. To minimize the energy over each section for a given active force, we take advantage of the small value of ε and expand the inner variables a, p, and the potential V to obtain the associated strain-energy density. Since the Euler-Lagrange equations and the boundary conditions are satisfied at each order, we can obtain solutions for the elastic strains at zero order $\mathbf{a}^{(0)}$ and at first order $\mathbf{a}^{(1)}$. Finally, these solutions which will represent a combination of bending and torsional deformation, will last for the duration of a muscle contraction as the actomyosin continues its contractile activity. The evaluation of the elastic energy under actomyosin muscle activity of order ε^4 can be compared with the equivalent energy of an extensible elastic rod and any fundamental deformation will be identified (Kirchhoff and Hensel (1883); Mielke (1988); Mora and Müller (2002, 2004); ***Moulton et al. (2020a)***). The typical quantities of interest are the curvature achieved during a bending event or a torsion as well as the total elongation ζ. In the *C. elegans* embryonic system, these quantities result from the competition between the active strains due to muscles and the myosin motors and the elasticity of the body. Similar active matter can be found in biological systems, from animals to plants, as illustrated in **Fig.4(A)-(C)**, they have a structure that generates internal stress/strain for the growth or daily activities. By combining anatomy and measurement techniques, we can transform the mechanics of the body under study into a soft sample subjected to localized internal active stresses or localized internal active strains and then deduce its overall deformation mechanisms, some examples are presented in **Fig.4(D)-(F)**.

The early elongation induced by the actomyosin

Experimental measurements during the early elongation stage reveal the embryonic diameter and the active or passive stresses, estimated by the opening of fractures realized in the body by laser ablation (***Vuong-Brender et al. (2017a)***; Ben Amar et al. (2018)). These quantities vary with the elongation. While previous studies have extensively investigated this initial stage, we have chosen to revisit it in the context of our geometry, with the goal of achieving complete control over our structural modeling, which includes the geometry, shear modulus, and activity of the actomyosin

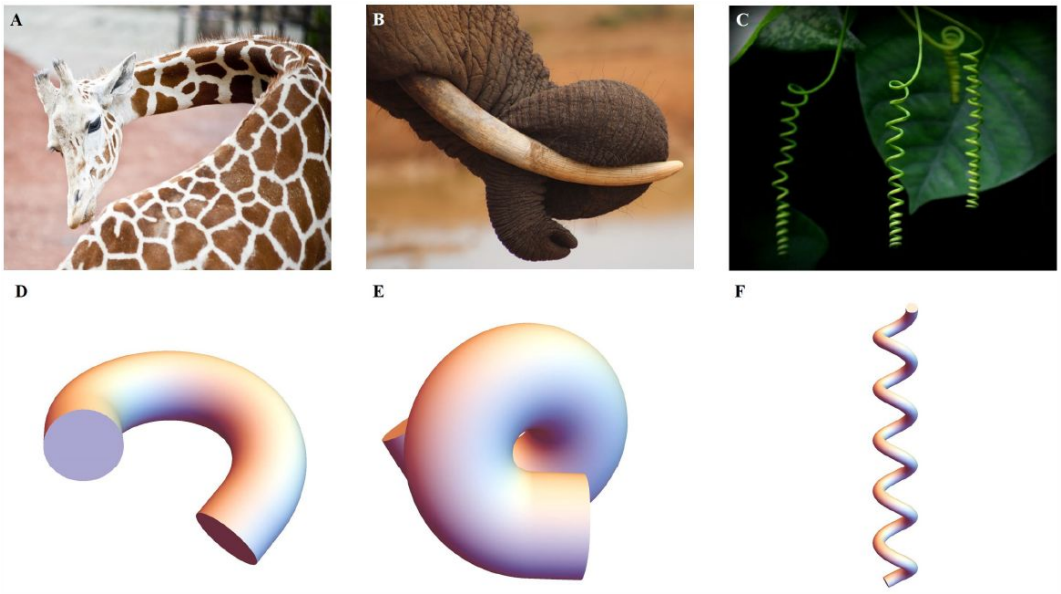

Figure 4.

(A) Bending of a giraffe's neck. (B) Torsion of an elephant's trunk. (B) Twisting of a plant vine. (D) to (F) Deformation configuration under different activations obtained by our simulations for bending and torsion of large rods, twisting and torsion of thin rods.

prior to muscle contraction. At the beginning of the second stage, the embryo experiences a pre-strain due to the early elongation, which we describe in our model as $\mathbf{G}_0$. The geometry and mechanical information are depicted in **Fig.5(A)**.

Here, we must first accurately determine $\mathbf{G}_0$ by analyzing the experimental data (***Vuong-Brender et al. (2017a)***; Ben Amar et al. (2018)). The cylinder can be divided into three distinct sections: the outer layer is the actin cortex, the thin ring where actin bundles concentrate and work, located within a radius range between R_2' and R_3 (as shown in **Fig.5(A)**); the middle layer ($R_2 < R < R_2$'), which is the epidermis but without actin; and the inner part ($0 < R < R_2$), where the muscle is located, along with some internal organs, tissues, and fluids. So, we treat the outer and middle layers as incompressible, but the inner part as a compressible material, except for the muscles. The initial deformation gradient: $\mathbf{F}_0$ =Diag($r'(R)$, $r(R)/R$, λ), and $\mathbf{G}_0$ = Diag(1, g_0, 1) with $0 < g_0 < 1$ in the actin layer, but with $g_0 = 1$ in the part without actin. $\mathbf{G}_0$ represents the circumferential strain exerted by actin during the early elongation and is a slowly varying function of time. By applying the principles of radius continuity, radial stress continuity, and incorporating the zero traction condition on the face of the cylinder, we can determine that $g_0 = 0.88$ when the elongation $\lambda = 1.8$, at the end of the early elongation. As illustrated in **Fig.5(B)**, the results of our model and the experimental data are in good agreement, demonstrating the consistency of the geometric and elastic modeling together with the choice of a pre-strain represented by $\mathbf{G}_0$ which gives a good prediction of the early elongation. More details can be found in the appendix 3.

From the first stage elongation represented by the blue dots and the blue dashed line in **Fig.5(C)** we can extract the time evolution of the contractile pre-strain $g_0(t_i)$ derived from our elastic model. To explain $g_0(t)$ quantitatively, we propose a phenomenological dynamical approach for the population of active myosin motors. This equation takes into account the competition between the recruitment of new myosin proteins from the epidermal cytoskeleton, which is necessary to elongate the embryo, and the detachment of these myosins from the actin cables, which is damped by the compressive radial stress. It reads:

$$\frac{dX_g(t)}{dt} = \left(p_1 - p_2 X_g(t) e^{-p_3 X_g(t)}\right) \frac{t_v}{t_p} \tag{3}$$

where $X_g = 1 - g_0(t)$, p_1 is the ratio of the freely available myosin population to the attached ones divided by the time of recruitment (given in minutes), while p_2 is the inverse of the debonding time of the myosin motors from the cable: $p_2 = 6\ \text{min}^{-1}$. The debonding time increases (or decreases) when the actin cable is under radial compressive (or tensile) stress, see Appendix 3, **Eq. (35)**. τ_v is the viscoelastic time estimated from laser ablation fracture operated in the epidermis (***Vuong-Brender et al. (2017b)***): $t_v = 6S$ and τ_p is the time required to activate the myosin motors $t_p = 1200S$ (Howard and Clark (2002)). This equation is similar to the model derived by Serra *et al* (Serra et al. (2021)) for the viscous stress that occurs during gastrulation.

Note that only p_1 and p_3 need be obtained by comparing $g_0(t)$ deduced from Eq.(3) with the values derived from our elastic model. The result of Eq.(3) with $p_1 = 0.6$ and $p_3 = 0.75$ are shown in **Fig.5(C)** with a rather good agreement.

Shape of the embryo under muscles and actomyosin contraction

The experimental regulation of muscle contraction in *C. elegans* (Yang (2017)) suggests a cyclic process in which two muscles on one side of the embryo contract quite at the same time and then stop, while on the opposite side the two muscles begin to contract, but with a delay. Let us first consider that only the muscles are active (see the schematic **Fig.6(A)** for the structure, then (B) and (C) for the bending). In this case, due to the geometry, bending to the left occurs when the left muscles are activated and then to the right for the symmetrical right muscles.

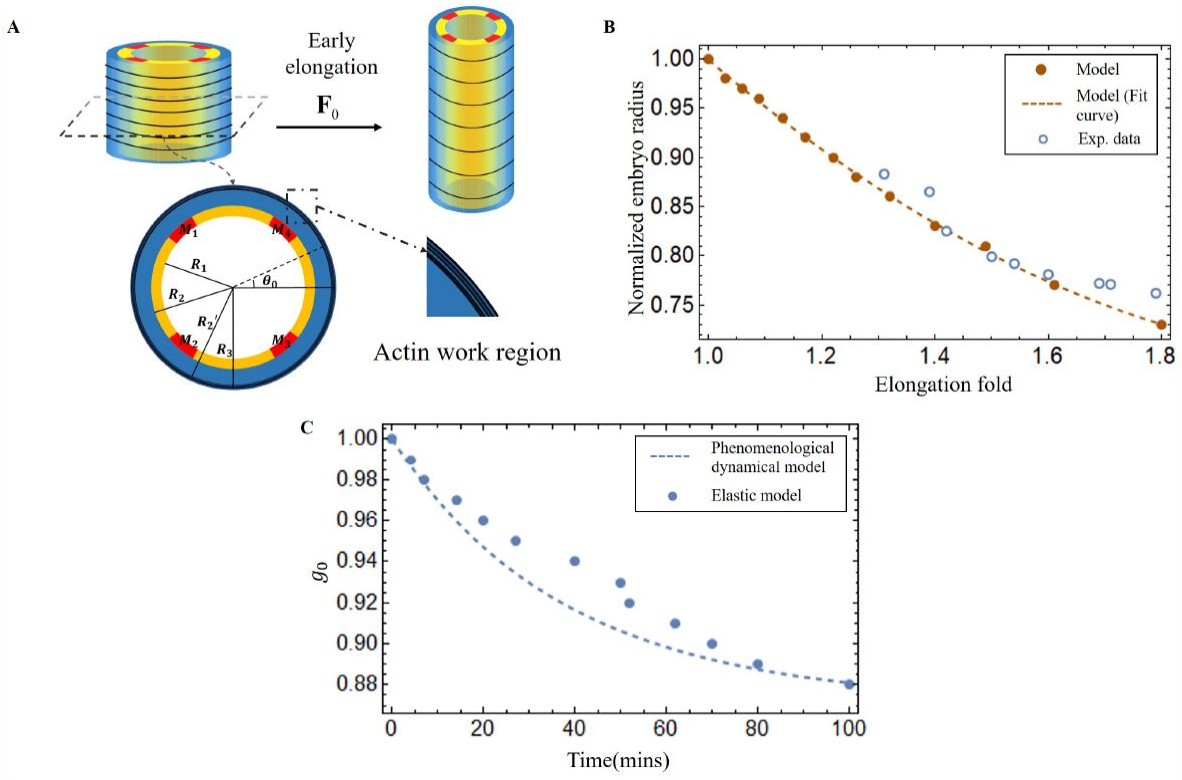

Figure 5.

(A) Schematic of early elongation and the cross section of *C. elegans*. In the cross-section, the black circular part is the actin region ($R_2' < R < R_3$, with shear modulus μ_a), the blue part is the epidermis layer ($R_2 < R < R_2'$ with shear modulus μ_e). The central or inner part ($0 < R < R_2$ in white has shear modulus μ_i, except for the four muscles, the shear modulus of the four muscles μ_m is much larger than the inner part. (B) Predictions of normalized embryo radius evolution during early elongation by the pre-strain model compared to experimental data from (***Vuong-Brender et al. (2017a)***). For the model, see **Eq.(20)** in Appendix 2. (C) Blue dots: extraction of the parameter $g_0(t)$ from **Eq.(30)** and **Eq.(32)** in Appendix 2. Blue dash line, see **Eq.(3)**.

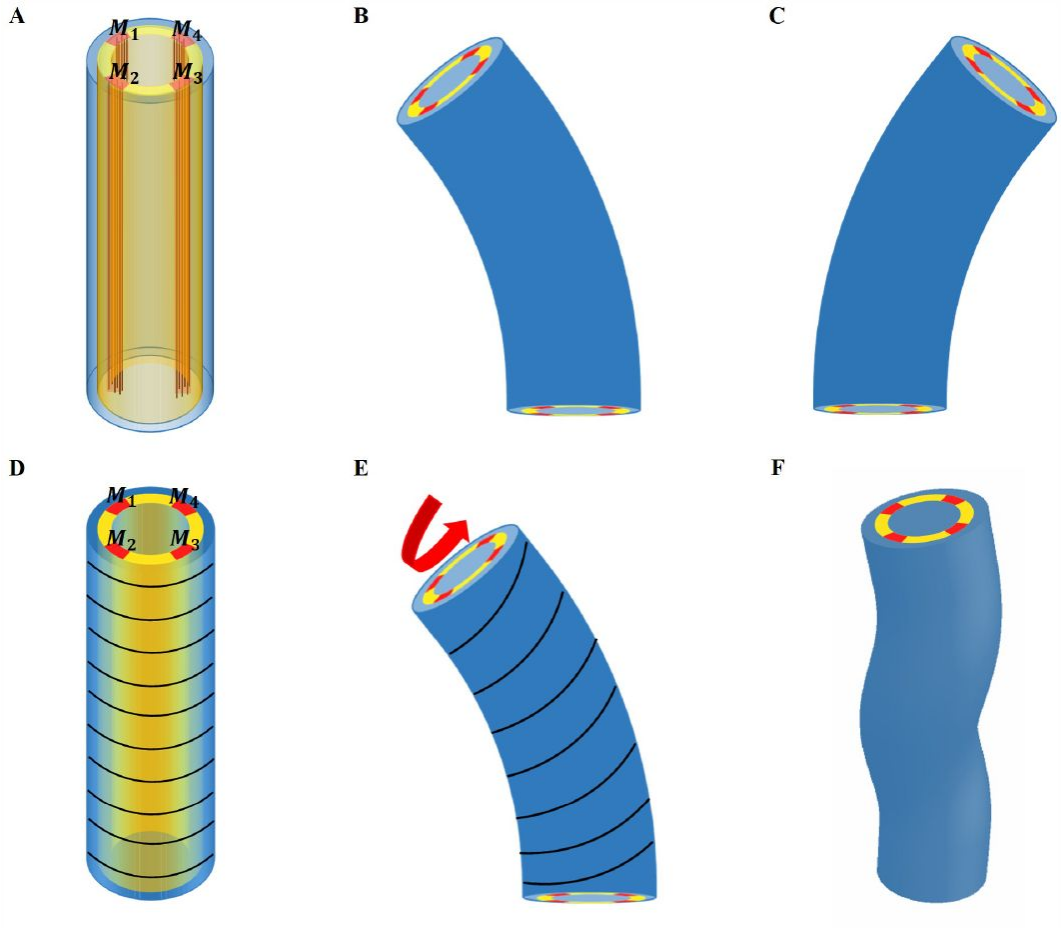

Figure 6.

(A) Schematic diagram of *C. elegans* muscle fibers and its cross section, and it does not show the actin fibers. There are four muscle bands exist in the yellow layer. However, the yellow region is not an actual tissue layer and it is only used to define the position of the muscles. (B) Deformation diagram, left side muscles M_1 and M_2 are activated. (C) Deformation diagram, right side muscles M_3 and M_4 are activated. (D) Schematic diagram of *C. elegans* actin fibers and cross section. (E) Once the muscle is activated, the actin fiber orientation changes from the 'loop' to the 'slope', resulting in torque. (F) Schematic diagram of torsional and bending deformation.

To be more quantitative, we assume that the left side muscles are activated during a short period with an active constant strain value g_m in the region M_1 and M_2, as shown in **Fig.6(A)-(B)**; if the muscles are perfectly vertical, $\alpha_m = \beta_m = 0$ in the initial configuration. In fact, the two muscles on the same side are not always completely in phase, and one may have a small delay. For simplicity, we assume that they contract simultaneously. During the entire initial period when the muscles are not activated, the actin fibers are distributed in a horizontal loop on the outer surface of the epidermis, but as soon as the muscle starts to contract, the actomyosin network will be reoriented (Lardennois et al. (2019)). The fibers are then distributed in an oblique pattern, which eventually causes the twisting of the embryo, see the schematic diagram in **Fig.6(D)-(F)**. When this region is activated with a constant strain value, g_a, the angle of the actin fibers will change according to the amplitude of the bending caused by the muscle contraction. In this situation, the angle of the actin fibers may change from $\alpha_a \in \left[0, \frac{\pi}{2}\right]$, but β_a is not changed and $\beta_a = 0$.

Throughout the entire process, the muscle and actomyosin activities are assumed to operate simultaneously. Our modeling allows us to evaluate the bending and torsion generated independently by muscles and actin bundles, culminating in a complete deformation under coupling. Furthermore, the angle of the actomyosin fibers varies during muscle contraction. We maintain a constant activation of the actomyosin network and gradually increase the muscle activation.

As a result, the structure will be bent, causing a change in the angle of the actin fibers, ultimately yielding a deformation map that is presented in **Fig.7(A)-(C)**. As myosin activation increased, we observed a consistent torsional deformation (**Fig.7(E)**) that agrees with the patterns seen in the video (**Fig.7(D)**). However, significant torsional deformations are not always present. In fact, other sources can induce torsion as a default symmetry of the muscle axis. We will now discuss torsion due to muscle contraction and the angle of deviation from the axis. In **Fig.7(F)-(G)**, we demonstrate that the curvature provided by the model increases with increasing muscle activation increases and that the torsion is not simply related to the activation amplitude, as it also depends on the value of the angle α_a, reaching a maximum at about $\pi/4$. Detailed calculations are given in Section Methods and Materials and Appendix 4.

Energy transformation and Elongation

During the late elongation process, the four internal muscle bands contract cyclically in pairs (Yang (2017); Williams and Waterston (1994)). Each contraction of a pair increases the energy of the system under investigation, which is then rapidly released to the body. This energy exchange causes the torsional bending energy to be converted into elongation energy, leading to an increase in length during the relaxation phase, as shown in **Fig.1** of the Appendix 5. With all the deformations obtained, **Eq.(2)** can be used to calculate the accumulated energy W_c produced by both the muscle and the actomyosin activities during a contraction. Subsequently, when the muscles on one side relax, the worm body returns to its original shape but with a tiny elongation corresponding to the transferred elastic energy. In this new state, the actin network assumes a 'loop' configuration with a strain of εg_{a1} once relaxation is complete. If all the accumulated energy from the bending-torsion deformation is used to elongate the worm body, the accumulated energy W_c and the energy W_r after muscle relaxation are equivalent. The activation of actin fibers g_{a1} after muscle relaxation can be calculated and determined by our model.

Once the first phase is well characterized, we can quantify the total energy resulting from both muscle and actomyosin after each contraction. We then used our model to predict elongation in wild type *C. elegans*, unc-112(RNAi) mutant and spc-1(RNAi) pak-1(tm403) mutant and further compared the results with experimental observations. The wild-type length increases from about 90 μm to 210 μm during the muscle-activated phase (Lardennois et al. (2019)), the phase lasts about 140 minutes, and the average time interval between two contractions is about 40 seconds

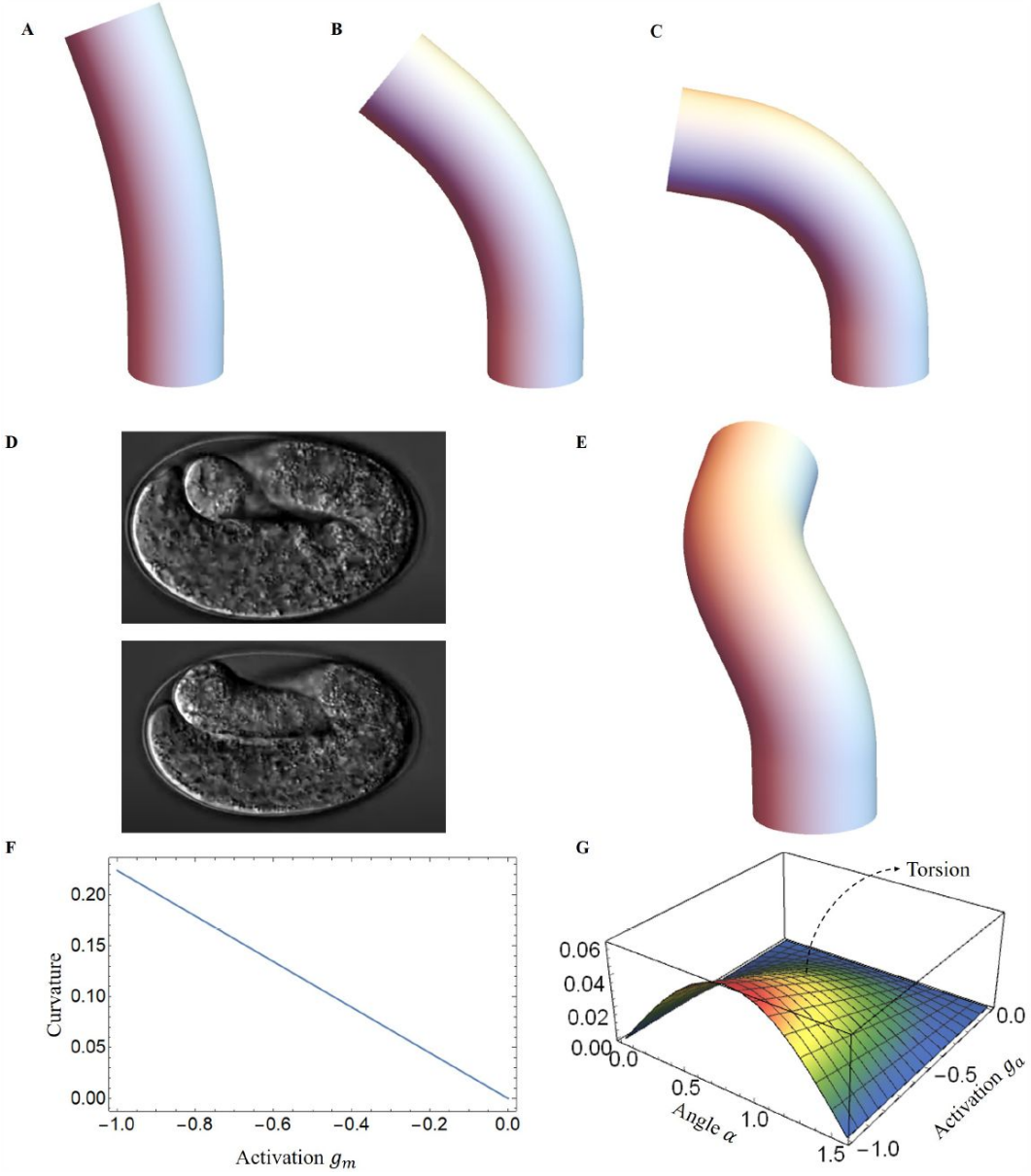

Figure 7.

Deformed configurations for different activation for muscles, (A) $g_m = -0.02$, $\alpha_a = \pi/3$, $g_a = -0.01$. (B) $g_m = -0.05$, $\alpha_a = \pi/4$, $g_a = -0.01$. (C) $g_m = -0.08$, $\alpha_a = \pi/6$, $g_a = -0.01$. (D) The graphs were captured from the Hymanlab, and the website: *https://www.youtube.com/watch?v=M2ApXHhYbaw*. The movie was acquired at a temperature of 20^0C using DIC optics. (E) $g_m = -0.1$, $\alpha_a = \pi/4$, $g_a = -0.7$. (F) Curvature is plotted as a function of muscle activation. (G) Torsion is plotted as a function of the actin activation and angle of actin fibers.

(Yang (2017)), so the number of contractions can be estimated to be about 210 times. Unfortunately, due to the difficulty of performing quantitative experiments on an embryo that is constantly moving in the egg shell between bending, torsion, and even rotations around its central axis, one can hypothesize this scenario: at each step i between the state $A_{i,0}$ to $A_{i,1}$ and then $A_{i,2}$, the whole mechanical muscle-myosin energy is transferred to the elongated step $A_{i,2}$, resulting a small $\delta\zeta_i$.

Considering the experimental results shown in **Fig.8(B)**, we determine the optimal values for the activation parameters: $g_m = -0.15$ and $g_a = -0.01$ assuming that all the energy accumulated during the muscle activation is transferred to the elongation process ($W_r = W_c$). The elementary elongation $\delta\zeta_i$ is gradually increased over time, which is shown as the black line in **Fig.8(A)**. At the beginning, $\delta\zeta_i$ is about $0.5\mu m$, but at the end of this process, $\delta\zeta_i$ is about $1.5\mu m$, indicating that the worm will grow up to $290\mu m$. The result is significantly larger than our actual size $210\mu m$. As the elongation progresses, we assume that there is an energy transfer between bending-torsion-contraction and elongation but it may not be fully effective, meaning that a significant part of the energy is lost. From the experimental data, we estimate that the energy loss gradually increases, from full conversion at the beginning to only 40% of the accumulated energy used for elongation at the end of the process ($W_r = 0.4W_c$). For $\delta\zeta_i$ it induces a first increase and then a decrease, which is shown as the blue line in **Fig.8(A)** and is responsible for the slowdown around 200 mins. This possibility, which may be not the only possible one, leads to the estimated elongation being in good agreement with the experimental data (see the blue-dashed curve in **Fig.8(B)**). Indeed it is possible that the *C. elegans* elongation requires other transformations that cost energy. As the embryo gradually elongates, energy dissipation and the biomechanical energy required to reorganize the actin bundles may be two factors contributing to the increased energy loss underlying the hypothesis.

In addition, it has been reported in (Norman and Moerman (2002)) that the knockdown of unc-112(RNAi), known the to affect muscle contractions, leads to the arrest of elongation of the embryos at the twofold stage, indicating that the muscles have no activation, $g_m = 0$ in our model, and no accumulated energy can be converted into elongation. Another mutation affecting the embryos consisting of mutant cells with pak-1(tm403), known to regulate the activity of myosin motors leads to a retraction of the embryo, so that the pre-stretch caused by myosin is not maintained and decreases. The results are fully consistent with a number of experimental observations and are shown in **Fig.8(B)**.

Embryo rotations and dissipation

The main manifestation of the muscle activity, independent of the elongation, is probably the constant rotation of the embryo despite its confinement in the egg. This can be explained by a small angular deviation of the muscle sarcomeres from the central axis due to their attachment to the inner boundary of the cell epidermis, the so-called “dense bodies” (Moerman and Williams (2006)). Since they cross the horizontal plane at about ±45° and the deviation β_m from the anterior-posterior axis is estimated to be about 6° each active muscle on the left (or on the right) contributes to the torque via a geometric factor of about $a_g = \sin(6\pi/180)\cos(\pi/4)$. Then a simple estimate of muscle activity in terms of torque is $\Lambda_m \sim \mu_m \pi R^3 S_m p_m a_g(\varepsilon g_m)$ where S_m is the area of the left or right muscle pair compared to the section of the cylinder: $S_m = 0.025$ and p_m is the distance of the muscles from the central axis of the embryo: $p_m = 0.75$ while $g_m = 0.15$ according to the elongation analysis. So the muscles on one side contribute to a torque Λ_m along the symmetry axis, given by $\Lambda_m = 4.657\mu_m \pi R^3 \cdot 10^{-5}$.

Let us now consider the dissipative torque, assuming that the rotational dynamics are stopped by friction after a bending event. Two cases can be considered: either the dissipation comes from the viscous flow or from the rubbing of the embryo when it folds. The fluid dissipation results from the rotations in the interstitial fluid inside and along the eggshell as the anterior-posterior axis remains parallel to the eggshell (***Bhatnagar et al. (2023)***) The interstitial fluid, of viscosity η

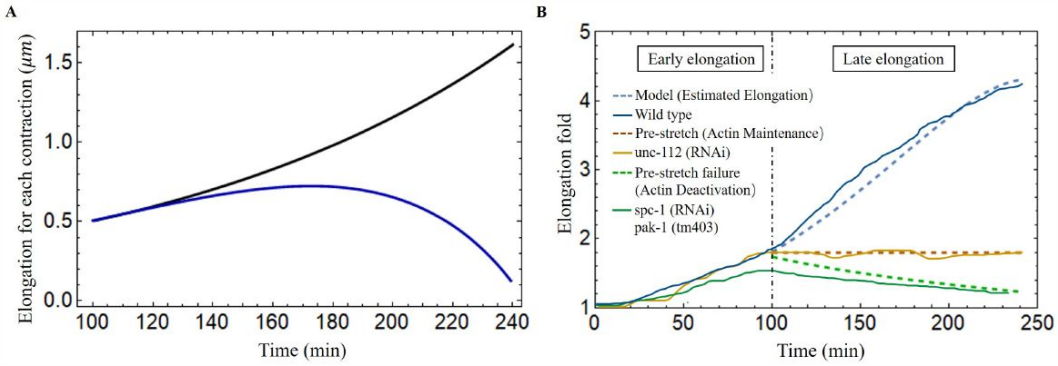

Figure 8.

(A) The elongation for each contraction varies with time. Black line: all energy converted to the elongation, blue line: partial energy converted to the elongation. The activation: g_m = −0.15, g_a = −0.01. (B) The model predicted results agree well with the experimental data of wild-type and different mutant *C. elegans* embryos (Lardennois et al. (2019)). Activation of the wild-type model (blue dashed line): g_m = −0.15, g_a = −0.01. The activation of unc-112(RNAi) (brown dashed line): g_m = 0, g_a = 0. In the case of pre-stretch failure (green dashed line), λ decreases from 1.8.

contains a significant amount of sugars and other molecules necessary for embryo survival and that is more viscous than water (Labouesse (2023)). However, values for sucrose or sorbitol at the concentration of 1 mole/liter indicate a viscosity on the order of a few times the viscosity of water, which is 1 mPas. For example at 0.9 mole/liter and temperature of 20°, an aqueous solution of sorbitol has a viscosity of 1.6 mPas, which can be extrapolated to η = 1.9 mPas at 1.2 mole/liter (Jiang et al. (2013)). The estimate given by an embryo located in the middle of the egg shell, gives a weaker viscous torque once evaluated by $\Lambda_v = 4\pi\eta\Omega_e L R^2 \left(R_{egg}^2/(R_{egg}^2 - R^2)\right)$ according to a classical result reported by Landau *et al.* (Landau and Lifshitz (1971, 2013)).

It should be noted that this estimation assumes that the two cylinders: the egg shell and the embryo have the same axis of symmetry and concerns the beginning of the muscle activity where the radius is about 8.2 μm, the length is 90 μm, the radius of the shell is about R_{egg} = 15μm and the length L_{egg} = 54μm, see **Fig.7(D)**. The angular velocity Ω_e is more difficult to evaluate but it is about 90° per two seconds deduced from videos. As the embryo approaches the eggshell, the friction increases, and two eccentric cylinders of different radii must be considered with the two symmetry axes separated by a distance *d*. The hydrodynamic study in this case is far from being trivial, and seems to have been first initiated by Zhukoski (Zhukoski (1887)), who proposed the use of bipolar coordinates for the mathematical treatment. Many subsequent papers were published after, using barious simplified assumptions, and the study was completely revisited by Ballal and Rivlin (Ballal and Rivlin (1976)). Here we focus on the limit of a small gap δ between the rotating body shape and the egg and by considering an asymptotic analysis at small δ of the general result derived in (Ballal and Rivlin (1976)). Thus, the viscous torque reads $\tilde{\Lambda}_v = 2\sqrt{2}\pi\eta\Omega_e L_c R_{egg}^2 \sqrt{R_{egg}/\delta}\sqrt{(R_{egg} - d)/d}$ where L_c is the zone of contact with the egg and d = R_{egg} −δ −R. This approach is an approximation since the embryo is more toroidal than cylindrical (Yang Xinyi et al. (2023)), but the evaluation of the dissipation is satisfactory for δ = 0.5μm, $\Omega_e \sim \pi/4\ S^{-1}$ and $\mu = 10^5 P\ a$. Going back back to the first model of dissipation with the same data, the ratio between the dissipative viscous torque and the active one gives: Λ_v/Λ_m = 0.02, which is obviously unsatisfactory. Finally, the dissipative energy $\mathcal{E}_{diSS}$ during one bending event leading to an angle of $\pi/2$ is $\mathcal{E} = 1/2\Lambda_m \times(\pi/2)^2$ which represents 4% of the muscle elastic energy during the bending so at the beginning of the muscle activity (Appendix 5, Eq.(45)), the dissipation is present but is negligible. At the very end of the process, this ratio becomes 60% but as already mentioned, our estimate for the dissipation becomes very approximate, increases a lot due to the embryo confinement, and does not include the numerous biochemical steps necessary to reorganize the active network: actomyosin and muscles.

Discussion

Since the discovery of the pre-embryonic muscle activity in the *C. elegans* embryo, it has become critical to explain the role of mechanical forces generated by muscle contraction on the behavioral and functional aspects of the epidermis. We provide a mechanical model in which the *C. elegans* is simplified as a cylinder, and the muscle bands and actin that drive its elongation are modeled as active structures in a realistic position. We determine the fiber orientation from experimental observations and then calculate the deformation by tensorial analysis using the strains generated by the active components. Although a special focus is given to late elongation, its quantitative treatment cannot avoid the influence of the first stage of elongation due to the actomyosin network, which is responsible for a pre-strain of the embryo. In a finite elasticity formalism, the deformations induced by the muscles in a second step are coupled to the level of strains of the initial elongation period. For this, we must revisit the theory of the actomyosin contraction and previous results (Ciarletta et al. (2009); ***Vuong-Brender et al. (2017a)***; Ben Amar et al. (2018)) to unify the complete treatment. In particular, a model for the recruitment of active myosin motors under forcing is presented that recovers the experimental results of the first elongation phase

The elongation process of *C. elegans* during the late period is much more complex than the early elongation stage which is caused by actin contraction alone. During late elongation, the worm is deformed by the combined action of muscle and actomyosin, resulting in an energy-accumulating process. Bending deformation is a phenomenon resulting from unilateral muscle contraction, and during the late elongation, significant torsional deformation is observed, indicating that the bending process induces a reorientation of the actin fibers. It should be noted that the embryo always rotates in parallel to the muscle activity, which makes any experimental measurements difficult. However, our model can predict that if the muscles are not perfectly vertical,a torque is generated that causes rotation and eventually torsion. The accumulated energy is then partially converted into energy for the ongoing action of actin, allowing the embryo to elongate when the muscle relaxes. Both sides of the *C. elegans* muscles contract in a sequential cycle, repeating the energy conversion process, and eventually completing the elongation process. However, the energy exchange between bending and elongation is limited, among other factors, by the viscous dissipation induced by rotation, which is also evaluated in this study. The necessary reorganization of the active networks (actomyosin and muscles) due to this enormous shape change of the embryo is not investigated here in detail. Parallel to the elongation, the cuticle is built around the body (Page and Johnstone (2007)). This very thin and stiff membrane provides protection and locomotion after hatching. Obviously, these processes will interfere with muscle activity. These two aspects, which intervene in the final stage of the worm's confinement, play a very important role at the interface between genetics, biochemistry, and mechanics.

Finally, the framework presented here not only provides a theoretical explanation for embryonic elongation in *C. elegans*, but can also be used to model other biological behaviors, such as plant tropism (***Moulton et al. (2020b)***) and elephant trunk elongation (***Schulz et al. (2022b***,a)) and bending. Our ideas could potentially be used in the emerging field of soft robotics, such as octopus leg inspired robots (Kang et al. (2012); Nakajima et al. (2013); Calisti et al. (2015)), which are soft and their deformation is induced by muscle activation. We can reliably predict the deformation by knowing the position of activation and the magnitude of fthe orces in the model. In addition, residual stresses can be incorporated into our model to achieve design goals.

Methods and Materials

The model has been presented in a series of articles by A. Goriely and collaborators (Goriely and Tabor (2013); Moulton et al. (2013, 2020b); Kaczmarski et al. (2022); Goriely et al. (2022)). As one can imagine, this is far from trivial, and most of the literature on the subject concerns either full cylinders or cylindrical shells in torsion around the axis of symmetry, the case of bending is far from trivial. However, the geometry of the muscles in *C. elegans* automatically leads to a bending process that cannot be discarded. We take advantage of these previous works and apply the methodology to our model.

The deformation gradient

The finite strain $\mathbf{G}_0$ maps the initial stress-free state $\mathcal{B}_0$ to a state $\mathcal{B}_1$, which describes the early elongation. We then impose an incremental strain filed $\mathbf{G}_1$ that maps the state $\mathcal{B}_1$ to the state $\mathcal{B}_2$, which represents late elongation. So, the deformation gradient can be expressed as: $\mathbf{F} = \mathbf{F}_e\mathbf{G}_1\mathbf{G}_0$ (Goriely and Ben Amar (2007)). The deformation gradient $\mathbf{F} = F_{ij}\,\mathbf{d}_i \otimes \mathbf{e}_j$, $i \in \{1, 2, 3\}$ and j labels the reference coordinates $\{R, \Theta, Z\}$ finally reads:

$$\mathbf{F} = \begin{bmatrix} a_{1R} & \frac{1}{R}a_{1\Theta} & \lambda\varepsilon\,(1+\varepsilon\xi)\,(u_2a_3 - u_3a_1\sin a_2) \\ a_1a_{2R} & \frac{a_1}{R}a_{2\Theta} & \lambda\varepsilon\,(1+\varepsilon\xi)\,(u_3a_1\cos a_2 - u_1a_3) \\ a_{3R} & \frac{1}{R}a_{3\Theta} & \lambda\,(1+\varepsilon\xi)\,(1+\varepsilon\,(u_1a_1\sin a_2 - u_2a_1\cos a_2)) \end{bmatrix}, \tag{4}$$

where λ is the axial extension due to the pre-strained.

We define $\mathbf{G}_0 = Diag\,(1, 1 + \varepsilon c, 1)$, since $g_0 = 0.88$ can be determined by the early elongation, we write it in the form of $1 + \varepsilon c$ to simplify the calculation, $c \approx -0.6$ ($\varepsilon \approx 0.2$).

Consider fibers oriented along the unit vector $\mathbf{m} = (\sin\alpha \sin\beta, \sin\alpha \cos\beta, \cos\alpha)$ for the incremental strain $\mathbf{G_1}$, where α and β characterize the angles with $\mathbf{e_z}$ and $\mathbf{e}_\theta$ and can be found in **Fig.3(A)**. The active filamentary tensor in cylindrical coordinates is then $\mathbf{G} = \mathbf{G}_0\,(\mathbf{I} + \varepsilon g\,\mathbf{m} \otimes \mathbf{m})$, see (Holzapfel (2000)) which reads:

$$\mathbf{G} = \mathbf{G_0} + \varepsilon g \mathbf{G_0} \begin{bmatrix} \sin^2\alpha\sin^2\beta & \sin^2\alpha \sin\beta\cos\beta & \sin\alpha\cos\alpha\sin\beta \\ \sin^2\alpha \sin\beta\cos\beta & \sin^2\alpha\cos^2\beta & \sin\alpha\cos\alpha\cos\beta \\ \sin\alpha\cos\alpha\sin\beta & \sin\alpha\cos\alpha\cos\beta & \cos^2\alpha \end{bmatrix}. \tag{5}$$

The energy function

The associated strain-energy density can be obtained by expanding the inner variables a_i (see Eq. (1)), p_i and the potential V (see Eq.(2)) as:

$$\mathbf{a} = \mathbf{a}^{(0)} + \varepsilon\mathbf{a}^{(1)} + \varepsilon^2\mathbf{a}^{(2)} + \mathcal{O}\left(\varepsilon^3\right), \tag{6}$$

$$p = p^{(0)} + \varepsilon p^{(1)} + \varepsilon^2 p^{(2)} + O\left(\varepsilon^3\right), \tag{7}$$

$$V(\mathbf{F}_e, \mathbf{G}) = V_0 + \varepsilon V_1 + \varepsilon^2 V_2 + O\left(\varepsilon^3\right). \tag{8}$$

For each cross section, the associated Euler-Lagrange equations take the following form:

$$\frac{\partial}{\partial R}\frac{\partial V_i R}{\partial a_{jR}^{(k)}} + \frac{1}{R}\frac{\partial V_i R}{\partial a_{jR}^{(k)}} + \frac{\partial}{\partial \Theta}\frac{\partial V_i R}{\partial a_{j\Theta}^{(k)}} - \frac{\partial V_i R}{\partial a_j^{(k)}} = 0, \tag{9}$$

where $j = 1, 2, 3$, $k = 0, 1$, in association with boundary conditions at each order $k = 0, 1$ on the outer radius R_i:

$$\left.\frac{\partial V_i R}{\partial a_{jR}^{(k)}}\right|_{R=R_i} = 0, j = 1, 2, 3. \tag{10}$$

We solve these equations order by order, taking incompressibility into account. At the lowest order, the incompressibility imposes the deformation: $\mathbf{a}^{(0)} = (r\,(R), \Theta, 0)$ and the Euler-Lagrange equation gives the Lagrange parameter $p^{(0)} = P_0(R)$ which finally read:

$$r' = \frac{R}{\lambda r},\ P_0' = 0, \tag{11}$$

and the boundary condition $\sigma_{rr}(R = 1) = 0$ gives the value of $P_0 = 1/\lambda$. At $\mathcal{O}(\varepsilon)$, the Euler-Lagrange equations are again automatically satisfied, and at $\mathcal{O}(\varepsilon^2)$, the crucial question is to get the correct expression for $a_i^{(1)}$ and $p^{(1)}$. Based on the previous subsection, the following form is intuited:

$$\begin{aligned} a_1^{(1)} &= -\frac{1}{2} r(R)\,\xi + q_1 r(R)^2 \left(u_1 \sin\Theta - u_2 \cos\Theta\right) + h_1(R) \\ a_2^{(1)} &= q_2 r(R) \left(u_1 \cos\Theta + u_2 \sin\Theta\right) + h_2(R) \\ a_3^{(1)} &= \lambda\xi \\ p^{(1)} &= h_3(R) \end{aligned} \tag{12}$$

As before, the Euler-Lagrange equations and the incompressibility condition give the two constants $q_1 = \frac{1}{8}\left(-2 + \lambda^3\right)$, $q_2 = \frac{1}{8}\left(2 + 3\lambda^3\right)$ and h_1, h_2, h_3 are a function of R. With the solutions for active strain $\mathbf{a}^{(0)}$ and $\mathbf{a}^{(1)}$, full expressions of them are given in the Appendix 4. The second order energy takes the form:

$$\mathcal{E} = \varepsilon^4 \int_0^L \mathrm{d}Z \int_S V_2\left(\mathbf{a}^{(0)}, \mathbf{a}^{(1)}; \mathrm{u}_1, \mathrm{u}_2, \mathrm{u}_3, \xi\right) R\mathrm{d}R\,\mathrm{d}\Theta + \mathcal{O}\left(\varepsilon^5\right), \tag{13}$$

and we can transform it into this form:

$$V_2 R = A_1\xi + A_2\xi^2 + B_1 u_1 + B_2 {u_1}^2 + C_1 u_2 + C_2 {u_2}^2 + D_1 u_3 + D_2 {u_3}^2, \tag{14}$$

where A_i, B_i, C_i and D_i are functions of R and Θ.

The method for determining deformation

Comparing with the energy of an extensible elastic rod (***Moulton et al. (2020a)***; Kirchhoff and Hensel (1883); Mielke (1988); Mora and Müller (2002, 2004)), we recognize the classic extensional stiffness K_0, bending stiffness K_1 and K_2, torsional stiffness K_3 coefficients:

$$K_0 = \int_{S_K} A_2 d\,R d\Theta,\ K_1 = \int_{S_K} B_2 d\,R d\Theta,\ K_2 = \int_{S_K} C_2 d\,R d\Theta,\ K_3 = \int_{S_K} D_2 d\,R d\Theta, \tag{15}$$

where A_2, B_2, C_2 and D_2 are related to the shear modulus μ, so for a uniform material with no variations of shear modulus, S_K represents the cross section of the cylinder. But if not, we need to divide different regions to perform the integration.

We now focus on the intrinsic extension and curvature of the cylindrical object induced by the active strains, which requires the competition of the active forces with the stiffness of the cylindrical beam according to the relationships,

$$\hat{\zeta} = 1 - H_0/K_0,\ \hat{u}_1 = -H_1/K_1, \hat{u}_2 = H_2/K_2,\ \hat{u}_3 = -H_3/K_3, \tag{16}$$

where H_i calculated by:

$$H_0 = \frac{1}{2}\int_{S_H} A_1 d\,R d\Theta,\ H_1 = \frac{1}{2}\int_{S_H} B_1 d\,R d\Theta,\ H_2 = \frac{1}{2}\int_{S_H} C_1 d\,R d\Theta,\ H_3 = \frac{1}{2}\int_{S_H} D_1 d\,R d\Theta. \tag{17}$$

where A_1, B_1, C_1 and D_1 are related to the shear modulus μ,the fiber angles α and β, and the activation g. So, the integration region S_H is divided into the different parts of the embryo which all contribute to the deformation.

To calculate the intrinsic Frenet curvature and torsion, we use the following equation:

$$\hat{\kappa} = \sqrt{\hat{u}_1^2 + \hat{u}_2^2} \quad \text{and} \quad \hat{\tau} = \frac{\hat{u}_3}{\hat{\zeta}}. \tag{18}$$

Finally, in the case of the activated left side muscles, we can calculate the intrinsic extension and curvatures using Eq.16), $\hat{u}_{1m} = 0$ and $\hat{u}_{3m} = 0$, so Frenet's intrinsic curvature and torsion Eq. (18), $\hat{\kappa}_m = \hat{u}_{2m}$ and $\hat{\tau}_m = 0$. For the activated actin case, we can calculate the intrinsic extension and curvatures by Eq.(16), $\hat{u}_{1a} = 0$ and $\hat{u}_{2a} = 0$, and the Frenet's intrinsic curvature and torsion Eq.(18), $\hat{\kappa}_a = 0$ and $\hat{\tau}_a = \frac{\hat{u}_{3a}}{\hat{\zeta}_a}$. These quantities have been used to calculate the deformation images, as shown previously in **Fig.7**.

After obtaining all solutions, we can use these quantities to calculate the accumulated energy W_c in the system after one contraction by **Eq.(2)**. By defining the activation (g_m and g_a) and the energy conversion efficiency, we can obtain the activation (g_{a1}) of the actin bundles after a single contraction and further calculate the elongation.

All calculation results and parameters are presented in the Appendix.

Acknowledgements

It is a pleasure to acknowledge fruitful discussions with Michel Labouesse and Kelly Molnar on experimental observations concerning the embryonic *C.elegans* elongation. We also thank Alain Goriely for his help with the technical aspects of nonlinear elasticity. Both authors acknowledge the support of the contract EpiMorph (ANR-2018-CE13-0008). Anna Dai acknowledges the support of the CSC (China Scholarship Council), file No. 201906250173.

Appendix 1 Size and material parameters

Appendix 2 Analytical model of the early elongation

The finite deformation gradient: $\mathbf{F}_0 = Diag(r'(R), r(R)/R, \lambda)$, and $\mathbf{G}_0 = Diag(1, g_0, 1)$, $0 < g_0 < 1$ in the actin layer, and $g_0 = 1$ in the part without actin bundles. To determine the finite strain $\mathbf{G}_0$, we converted the four muscle parts into thin layers attached to the epidermis in equal proportions to ensure the continuity of the model, and divided our model into four parts, see **Fig.1**. The actin layer($R_3 < R < R_2'$), epidermis layer($R_2 < R < R_2'$) and muscle layer($R_1' < R < R_2$) are considered as incompressible materials, and the inner part($0 < R < R_1'$) is compressible. The Neo-Hookean energy function is used for the incompressible parts:

$$W = \mu\left[\frac{1}{2}\left(Tr\left(\mathbf{F}_e\mathbf{F}_e^T\right) - 3\right) - q\left(\det \mathbf{F}_e - 1\right)\right], \tag{19}$$

Geometry parameters	Normalized radii[1]	R_1=0.7	R_2=0.8	R_2'=0.96	R_3=1
	The location of muscles[2]	$\theta_1=\frac{2}{3}\pi$ $\theta_2=\frac{5}{6}\pi$	$\theta_3=\frac{7}{6}\pi$ $\theta_4=\frac{4}{3}\pi$	$\theta_5=\frac{5}{3}\pi$ $\theta_6=\frac{11}{6}\pi$	$\theta_7=\frac{1}{6}\pi$ $\theta_8=\frac{1}{3}\pi$
Material parameters (Shear modulus)[3]	Actin part	$\mu_a=5$			
	Epidermis part	$\mu_e=1$			
	Muscles	$\mu_m=100$			
	Soft inner part	$\mu_i=1/200$			

[1] The radii are extracted or inferred from the Ref.(***Ben Amar et al.*** (***2018***); ***Lardennois et al.*** (***2019***)).
[2] The position and size of the muscles are inferred from the Ref.(***Moerman and Williams*** (***2006***); ***Lardennois et al.*** (***2019***)).
[3] The units of the shear modulus are the KPa and is scaled by the epidermis one. It gives for the muscle, a value consistent with the muscle shear modulus proposed in (***Denham et al.*** (***2018***)).

Appendix 1—table 1

Parameters adopted in this work

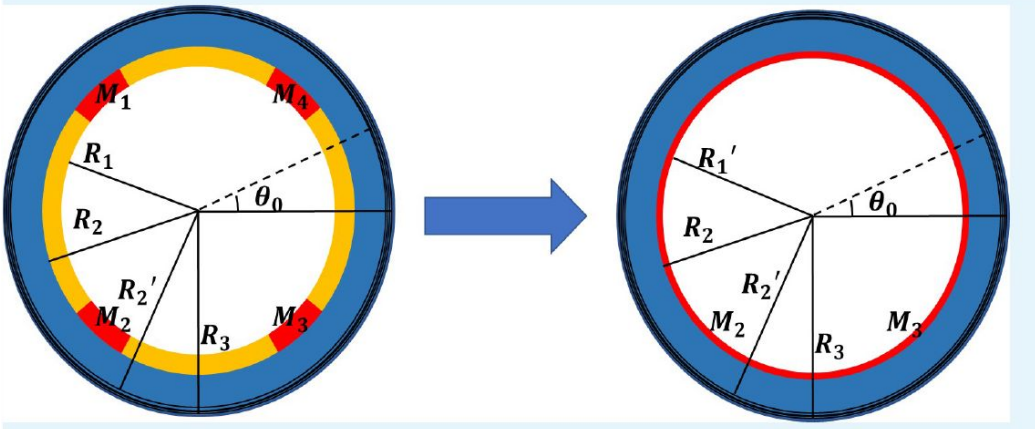

Appendix 2—figure 1.

Simplified ross-sectional model with four scattered muscle sections simplified to thin layers (R_1 = 0.7, R_1' = 0.768, R_2 = 0.7, R_2' = 0.96).

According to the Euler-Lagrange equations, we can obtain the radius of the actin layer(r_a), the epidermis layer(r_e), and the muscle layer(r_m):

$$r_a = \sqrt{\frac{g_0 R^2 + A}{\lambda}}, \quad r_e = \sqrt{\frac{R^2 + E}{\lambda}}, \quad r_m = \sqrt{\frac{R^2 + M}{\lambda}}. \tag{20}$$

where A, E and M are constants, and the Lagrange multiplier q in the actin, epidermis and muscle layers:

$$q_a = \frac{-\log(R) + \frac{1}{2}g_0{}^2\left(-\frac{A}{A+g_0R^2} + \log\left(A + g_0R^2\right)\right)}{g_0\lambda} + C_a, \tag{21}$$

$$q_e = -\frac{\frac{E}{E+R^2} + 2\log(R) - \log\left(E + R^2\right)}{2\lambda} + C_e, \tag{22}$$

$$q_m = -\frac{\frac{M}{M+R^2} + 2\log(R) - \log\left(M + R^2\right)}{2\lambda} + C_m. \tag{23}$$

For the compressible part, we take the energy function form (Holzapfel (2000)):

$$W = \frac{\mu}{2}\left(Tr\left(\mathbf{F_e}\mathbf{F_e}^T\right) - 3 + \kappa\left(\det \mathbf{F_e} - 1\right)^2\right) \tag{24}$$

where κ is a material constant. The radius of the inner part is:

$$r_i = \frac{aR}{\sqrt{\lambda}} \tag{25}$$

where a is a constant.

By considering the boundary condition $\sigma_{rr} = 0$ on the outer border $R = 1$:

$$\sigma_{arr}(R=1) = \mu_a\left[\left(\frac{\partial r_a(1)}{\partial R}\right)^2 - q_a(1)\right] = 0 \tag{26}$$

the continuity of the radius:

$$r_a\left(\mathrm{R}_2'\right) = r_e\left(\mathrm{R}_2'\right), \quad r_e\left(\mathrm{R}_2\right) = r_m\left(\mathrm{R}_2\right), \quad r_m\left(\mathrm{R}_1'\right) = r_i\left(\mathrm{R}_1'\right), \tag{27}$$

and the continuity of the radial stresses σ_{rr} in R_2' and R_2 :

$$\mu_a\left[\left(\frac{\partial r_a\left(\mathrm{R}_2'\right)}{\partial R}\right)^2 - q_a\left(\mathrm{R}_2'\right)\right] = \mu_e\left[\left(\frac{\partial r_e\left(\mathrm{R}_2'\right)}{\partial R}\right)^2 - q_e\left(\mathrm{R}_2'\right)\right], \tag{28}$$

$$\mu_e\left[\left(\frac{\partial r_e\left(\mathrm{R}_2\right)}{\partial R}\right)^2 - q_e\left(\mathrm{R}_2\right)\right] = \mu_m\left[\left(\frac{\partial r_m\left(\mathrm{R}_2\right)}{\partial R}\right)^2 - q_m\left(\mathrm{R}_2\right)\right]. \tag{29}$$

Using the above equations, we can obtain expressions for the constants E, M, C_a, C_e and C_m.

We replace all size and material parameters and $\kappa = 100$, $\lambda = 1.8$ in the last condition $\sigma_{mrr}(R_1') = \sigma_{irr}(R_1')$

$$\mu_m\left[\left(\frac{\partial r_m(R_1')}{\partial R}\right)^2 - q_m(R_1')\right] = \mu_i \sigma_{irr}(R_1'), \tag{30}$$

where σ_{irr}:

$$\sigma_{irr} = \frac{2}{\det \mathbf{F}_e}\left((\det \mathbf{F}_e)^2 \frac{\partial W}{\partial(\det \mathbf{F}_e)^2} + \frac{\partial W}{\partial(tr(\mathbf{F}_e \mathbf{F}_e^T))} r_i'(R)^2\right). \tag{31}$$

and obtain the relation with constant A and g_0.

Finally, by prescribing a zero traction condition on the top of the cylinder, the muscle part was noticeably considered inextensible, so there was no stress on the top:

$$\int_{R_2'}^{1} \sigma_{azz} r_a r_a' dR + \int_{R_2}^{R_2'} \sigma_{ezz} r_e r_e' dR + \int_{0}^{R_1'} \sigma_{izz} r_i r_i' dR, \tag{32}$$

where:

$$\sigma_{azz} = \lambda^2 - q_a, \quad \sigma_{ezz} = \lambda^2 - q_e, \tag{33}$$

$$\sigma_{izz} = \frac{2}{\det \mathbf{F}_e}\left((\det \mathbf{F}_e)^2 \frac{\partial W}{\partial(\det \mathbf{F}_e)^2} + \frac{\partial W}{\partial(tr(\mathbf{F}_e \mathbf{F}_e^T))} \lambda^2\right), \tag{34}$$

all solutions $g_0 = 0.88$, $A = 0.08$ and $r_a(1) = 0.73$ can be determined. The result is also in good agreement with the experimental data (***Vuong-Brender et al. (2017a)***; Ben Amar et al. (2018)).

Appendix 3 Time-scale for myosin detachment

The time required for non-muscle myosin detachment is estimated to be $\tau_0 = 10S$ for free actomyosin filaments. If the actin filament is subjected to an external load perpendicular to its axis, detachment can be facilitated, or on the contrary, inhibited, see (Howard and Clark (2002)), page 169-170. In the present case, the stresses acting in the radial direction of an actin bundle are compressive and thus will retard the detachment. This energy must be compared to the energy of detachment of all myosin motors from the bundle. The corresponding elastic energy associated with the radial deformation for an actin cable of length l_a with radius $r_b = 0.05\mu m$ estimated from (Lardennois et al. (2019)) and shear modulus $\mu_a = 5\ KP\ a$ is given by $1/2\mu_a(1 - g_0(t))\pi l_a r_b^2 = 210^{-11} l_a\ J$. This result must be compared to the individual energy of detachment times the number of myosin motors on a cable. This number is difficult to determine but an estimate is given by the length of the cable l_a divided by the distance between 2 myosin anchoring sites, which is about $5nm$ while the attachment energy per motor is about $6k_bT$. These values are for skeletal muscle myosins (Howard and Clark (2002)) and must be taken with caution. Nevertheless, the order of magnitude of the detachment energy for a collection of myosin

heads from actin cable can be estimated to be $4.8 l_a 10^{-12} J$. Then the ratio between the two quantities is of the order $4(1 - g_0(t))$, which explains that the time scale of debonding for a cable under compressive stress in the direction orthogonal of its axis is then:

$$\tau_{deb} = \tau_0 e^{p_3(1-g_0(t))} \tag{35}$$

where p_3 is a positive constant of order one that cannot be predicted exactly. This time scale justifies the exponential correction in Eq.(3) of the manuscript.

Appendix 4 Modelling in the absence of pre-strain

The paper discusses the case with pre-strain. Here, are more details about the case without pre-strain ($\mathbf{G_0} = \mathbf{I}$). Up to the lowest order, the solution of the Euler–Lagrange equations is obviously given by $\mathbf{a}^{(0)} = (R, \Theta, 0)$, and $p^{(0)} = 1$, so there is no deformation and the zero and first order energies vanish. At order $\mathcal{O}(\varepsilon^2)$ of the elastic energy, the solutions for the active strain components are

$$\begin{aligned}
a_1^{(1)} &= -\frac{R}{2}\xi - \frac{R^2}{8}\left(u_1 \sin\Theta - u_2 \cos\Theta\right) + f_1(R), \\
a_2^{(1)} &= \frac{5R}{8}\left(u_1 \cos\Theta + u_2 \sin\Theta\right) + f_2(R), \\
a_3^{(1)} &= 0, \\
p^{(1)} &= f_3(R).
\end{aligned} \tag{36}$$

where $f_{1,2}$ are functions related to the active stress g and the fiber angles α and β:

$$\begin{aligned}
f_1(R) &= \frac{gR}{2}, \\
f_2(R) &= glog(R)\sin^2\alpha \sin(2\beta), \\
f_3(R) &= 2g\mu log(R)\sin^2\alpha \sin(2\beta).
\end{aligned} \tag{37}$$

The stiffness coefficients :

$$\begin{aligned}
A_2 &= \frac{9\mu R}{8}, \\
B_2 &= \frac{81}{128}\mu R^3 \sin^2\Theta, \\
C_2 &= \frac{81}{128}\mu R^3 \cos^2\Theta, \\
D_2 &= \frac{\mu R^3}{2}.
\end{aligned} \tag{38}$$

The deformation coefficients :

$$\begin{aligned}
A_1 &= -\frac{1}{8}g\mu R\left[4 + 5\cos(2\alpha) + 2\cos(2\beta)(-1 + 2\log(R))\sin^2\alpha\right], \\
B_1 &= -\frac{1}{16}g\mu R^2\left[10 + 17\cos(2\alpha) + 2\cos(2\beta)(-1 + 14\log(R))\sin^2\alpha\right]\sin\Theta, \\
C_1 &= \frac{1}{16}g\mu R^2\left[10 + 17\cos(2\alpha) + 2\cos(2\beta)(-1 + 14\log(R))\sin^2\alpha\right]\cos\Theta, \\
D_1 &= -g\mu R^2 \cos\beta \sin(2\alpha).
\end{aligned} \tag{39}$$

Modelling with pre-strain

The first-order solutions of the theory with the case of pre-strain, $h_{1,2,3}(R)$, are related to the activation g and the fiber angles α and β:

$$\begin{aligned} h_1(R) &= \frac{R(c+g)}{2\sqrt{\lambda}}, \\ h_2(R) &= g\log(R)\sin^2\alpha\sin(2\beta), \\ h_3(R) &= \frac{2\mu log(R)\left[c+g\cos(2\beta)\sin^2\alpha\right]}{\lambda}. \end{aligned} \tag{40}$$

The stiffness coefficients are:

$$\begin{aligned} A_2 &= (0.278+1.689\mu)R, \\ B_2 &= 1.294R^3\left[-0.405+2.389\mu+(-0.176+\mu)\cos(2\Theta)\right], \\ C_2 &= -1.294R^3\left[0.405-2.389\mu+(-0.176+\mu)\cos(2\Theta)\right], \\ D_2 &= 0.9\mu R^3. \end{aligned} \tag{41}$$

The deformation coefficients are:

$$\begin{aligned} A_1 &= \mu R\left[0.417c-0.139g-6.48g\cos^2\alpha-0.556c\log(R)\right. \\ &\quad \left.+g\left(0.556\cos^2\beta-0.556\cos(2\beta)\log(R)\right)\sin^2\alpha\right]. \\ B_1 &= R^2\left\{g(-0.828+4.830\mu)\cos\beta\log(R)\sin^2\alpha\sin\beta\cos\Theta+0.198c\sin\Theta\right. \\ &\quad +\left[0.198g+0.910c\mu+1.307g\mu-4.830g\mu\cos^2\alpha-1.225c\mu\log(R)\right. \\ &\quad \left.\left.+g\mu\left(-0.397\cos^2\beta-1.225\cos(2\beta)\log(R)\right)\sin^2\alpha\right]\sin\Theta\right\}. \\ C_1 &= R^2\left\{g(-0.828+4.830\mu)\cos\beta\log(R)\sin^2\alpha\sin\beta\sin\Theta-0.198c\cos\Theta\right. \\ &\quad +\left[-0.198g-0.910c\mu-1.307g\mu+4.830g\mu\cos^2\alpha+1.225c\mu\log(R)\right. \\ &\quad \left.\left.+g\mu\left(0.397\cos^2\beta+1.225\cos(2\beta)\log(R)\right)\sin^2\alpha\right]\cos\Theta\right\}. \\ D_1 &= -g\mu R^2\cos\beta\sin(2\alpha). \end{aligned} \tag{42}$$

Appendix 5 Energy transformation calculations

The energy transformation process is depicted in **Fig.1**.

To obtain the elongation $\delta\zeta_i$ after each muscle contraction, we need to calculate the energy, and the total energy has the following form:

$$\mathcal{E} = \varepsilon^2\int_0^L dZ\int_S\left(V_0+\varepsilon V_1+\varepsilon^2V_2\right)R\,dR\,d\Theta+O\left(\varepsilon^5\right) \tag{43}$$

where the integration domain S refers to each part of the cylinder with a different shear modulus μ, so the model must be divided into 3 different parts for integration.

The final part is the energy conversion per unit volume:

$$\mathcal{E}_{\mp} = \int_S\left(\varepsilon V_1+\varepsilon^2V_2\right)R\,dR\,d\Theta \tag{44}$$

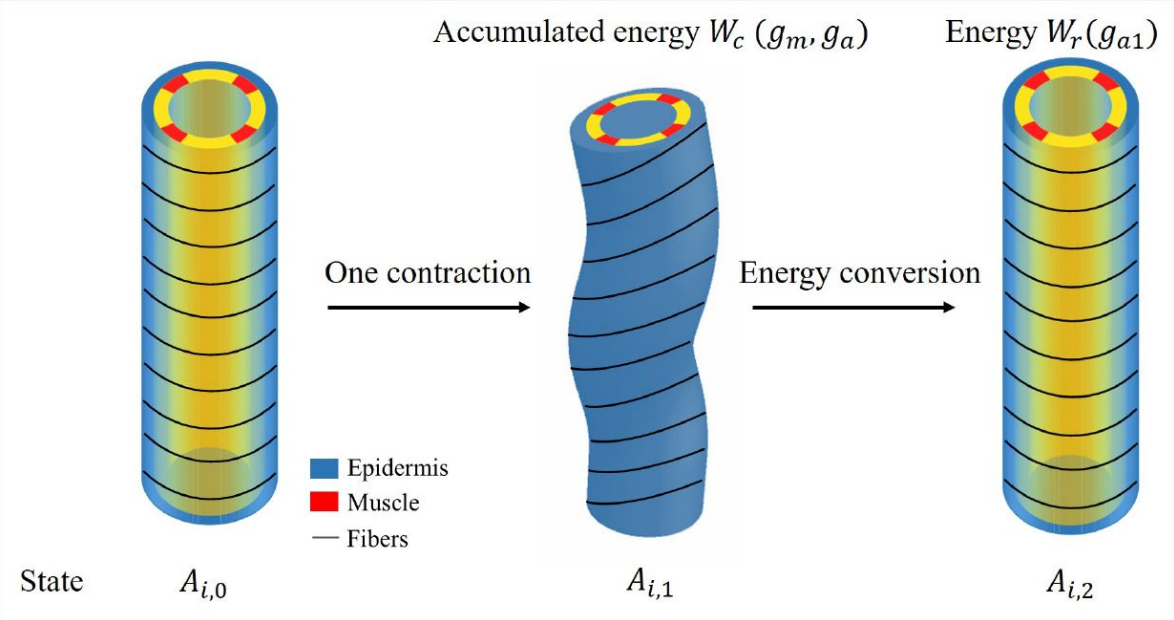

Appendix 5—figure 1.

Schematic diagram of energy conversion.

where V_1 is not the total first-order energy, we consider only the energy induced by the activation of actomyosin g_a and muscle g_m. After obtaining solutions $\mathbf{a}^{(0)}$,$\mathbf{a}^{(1)}$ and deformations from **Eq. (11)**-**(12)**, the accumulated energy during the contraction period W_c, which we define, is:

$$W_c = \int_S \left(\varepsilon V_1 + \varepsilon^2 V_2\right) R \, \mathrm{d}R \, \mathrm{d}\Theta = \varepsilon \left(-10.70 g_a - 7.73 g_m\right) + \varepsilon^2 \left[\left(-3.31 + 26.75 g_a\right) g_a + 11.95 {g_m}^2\right]. \tag{45}$$

When the muscles are relaxed and only actomyosin is activated, the total increase in volumetric energy is W_r:

$$W_r = \int_S \left(\varepsilon V_1 + \varepsilon^2 V_2\right) R \, \mathrm{d}R \, \mathrm{d}\Theta = -0.41 \varepsilon g_{a1} + \varepsilon^2 \left(-5.19 + 6.96 g_{a1}\right) g_{a1}. \tag{46}$$

By calculating the energy conversion, we obtain $g_{a1} = -0.66$ at the beginning of the late elongation phase, **Fig.7** of the manuscript shows the elongation for each contraction and total elongation varies with time.

References

Ballal B, Rivlin R. (1976) **Flow of a Newtonian fluid between eccentric rotating cylinders: inertial effects** *Archive for Rational Mechanics and Analysis* **62**:237–294

Ben Amar M, Bordner A. (2017) **Mimicking cortex convolutions through the wrinkling of growing soft bilayers** *Journal of Elasticity* **129**:213–238

Ben Amar M, Jia F. (2013) **Anisotropic growth shapes intestinal tissues during embryogenesis** *Proceedings of the National Academy of Sciences* **110**:10525–10530

Ben Amar M, Qiuyang-Qu P, Vuong-Brender TTK, Labouesse M. (2018) **Assessing the contribution of active and passive stresses in C. elegans elongation** *Physical Review Letters* **121**

Bertet C, Sulak L, Lecuit T. (2004) **Myosin-dependent junction remodelling controls planar cell intercalation and axis elongation** *Nature* **429**:667–671

Bhatnagar A, Nestler M, Gross P, Kramar M, Leaver M, Voigt A, Grill SW (2023) **Axis convergence in C. elegans embryos** *bioRxiv*

Blankenship JT, Backovic ST, Sanny JS, Weitz O, Zallen JA (2006) **Multicellular rosette formation links planar cell polarity to tissue morphogenesis** *Developmental cell* **11**:459–470

Bouchard A, Hofland GW, Witkamp GJ (2007) **Properties of sugar, polyol, and polysaccharide waterethanol solutions** *Journal of Chemical & Engineering Data* **52**:1838–1842

Calisti M, Corucci F, Arienti A, Laschi C. (2015) **Dynamics of underwater legged locomotion: modeling and experiments on an octopus-inspired robot** *Bioinspiration & biomimetics* **10**

Chadwick R. (1985) **Slow viscous flow inside a torus—the resistance of small tortuous blood vessels** *Quarterly of applied mathematics* **43**:317–323

Ciarletta P, Ben Amar M, Labouesse M. (2009) **Continuum model of epithelial morphogenesis during Caenorhabditis elegans embryonic elongation** *Philosophical Transactions of the Royal Society A: Mathematical, Physical and Engineering Sciences* **367**:3379–3400

Ciarletta P, Ben Amar M. (2012) **Papillary networks in the dermal–epidermal junction of skin: a biomechanical model** *Mechanics Research Communications* **42**:68–76

Coulombre AJ, Coulombre JL (1958) **Intestinal development: I. Morphogenesis of the villi and musculature** *Journal of Embryology and Experimental Morphology* **6**:403–411

Cowan CR, Hyman AA (2007) **Acto-myosin reorganization and PAR polarity in C. elegans** *Development* **134**:1035–1043

De Vita R, Grange R, Nardinocchi P, Teresi L. (2017) **Mathematical model for isometric and isotonic muscle contractions** *Journal of Theoretical Biology* **425**:1–10

Denham JE, Ranner T, Cohen N. (2018) **Signatures of proprioceptive control in Caenorhabditis elegans locomotion** *Philosophical Transactions of the Royal Society B: Biological Sciences* **373**

Gally C, Wissler F, Zahreddine H, Quintin S, Landmann F, Labouesse M. (2009) **Myosin II regulation during C. elegans embryonic elongation: LET-502/ROCK, MRCK-1 and PAK-1, three kinases with different roles** *Development* **136**:3109–3119

Goriely A. (2017) **The mathematics and mechanics of biological growth**

Goriely A, Ben Amar M. (2007) **On the definition and modeling of incremental, cumulative, and continuous growth laws in morphoelasticity** *Biomechanics and modeling in mechanobiology* **6**:289–296

Goriely A, Geers MG, Holzapfel GA, Jayamohan J, Jérusalem A, Sivaloganathan S, Squier W, van Dommelen JA, Waters S, Kuhl E. (2015) **Mechanics of the brain: perspectives, challenges, and opportunities** *Biomechanics and modeling in mechanobiology* **14**:931–965

Goriely A, Moulton DE, Mihai Angela (2022) **A rod theory for liquid crystalline elastomers** *Journal of Elasticity* :1–24

Goriely A, Tabor M. (2013) **Rotation, inversion and perversion in anisotropic elastic cylindrical tubes and membranes** *Proceedings of the Royal Society A: Mathematical, Physical and Engineering Sciences* **469**

Hannezo E, Prost J, Joanny JF (2011) **Instabilities of monolayered epithelia: shape and structure of villi and crypts** *Physical Review Letters* **107**

Hidayanto E, Tanabe T, Kawai J. (2010) **Measurement of viscosity and sucrose concentration in aqueous solution using portable Brix meter** *Berkala Fisika* **13**:23–28

Holzapfel GA (2000) **Nonlinear solid mechanics: a continuum approach for engineering science**

Howard J, Clark R. (2002) **Mechanics of motor proteins and the cytoskeleton** *Appl Mech Rev* **55**:B39–B39

Jiang X, Zhu C, Ma Y. (2013) **Density and viscosity of sorbitol/maltitol in L-ascorbic acid aqueous solutions at T=(293.15 to 323.15) K** *Journal of Molecular Liquids* **188**:67–73

Kaczmarski B, Moulton DE, Kuhl E, Goriely A. (2022) **Active filaments I: Curvature and torsion generation** *Journal of the Mechanics and Physics of Solids* **164**

Kang R, Branson DT, Guglielmino E, Caldwell DG (2012) **Dynamic modeling and control of an octopus inspired multiple continuum arm robot** *Computers & Mathematics with Applications* **64**:1004–1016

Kirchhoff G, Hensel K. (1883) **Vorlesungen über mathematische Physik**

Kücken M, Newell AC (2005) **Fingerprint formation** *Journal of theoretical biology* **235**:71–83

Labouesse M. (2023) **Viscosity of the interstitial fluid** *The fluid contained in the embryo egg is a highly viscous solution full of diverse sugars and other molecules necessary for metabolism The proof is given by the necessity to put the embryo in a solution when the hatching is achieved on purpose The survival of the embryo lasts few hours The solution is a sorbitol aqueous solution containing approximately 1-12 mole/L*

Landau L, Lifshitz E. (1971) **Mécanique des fluides**

Landau LD, Lifshitz EM (2013) **Fluid Mechanics: Landau and Lifshitz** *Course of Theoretical Physics*

Lardennois A *et al.* (2019) **An actin-based viscoplastic lock ensures progressive body-axis elongation** *Nature* **573**:266–270

Lesanpezeshki L, Qadota H, Darabad MN, Kashyap K, Lacerda CM, Szewczyk NJ, Benian GM, Vanapalli SA (2021) **Investigating the correlation of muscle function tests and sarcomere organization in C. elegans** *Skeletal muscle* **11**:1–15

Levayer R, Lecuit T. (2012) **Biomechanical regulation of contractility: spatial control and dynamics** *Trends in cell biology* **22**:61–81

Li B, Cao YP, Feng XQ, Gao H. (2011) **Surface wrinkling of mucosa induced by volumetric growth: theory, simulation and experiment** *Journal of the Mechanics and Physics of Solids* **59**:758–774

Lv C, Yang Y, Li B. (2022) **Nano/micromotors in active matter** *Micromachines* **13**

McKeown C, Praitis V, Austin J. (1998) **sma-1 encodes a betaH-spectrin homolog required for Caenorhabditis elegans morphogenesis** *Development* **125**:2087–2098

Mielke A. (1988) **On Saint-Venant's problem for an elastic strip** *Proceedings of the Royal Society of Edinburgh Section A: Mathematics* **110**:161–181

Moerman DG, Williams BD (2006) **Sarcomere assembly in C. elegans muscle** *WormBook: The Online Review of C elegans Biology*

Mora MG, Müller S. (2002) **Derivation of the nonlinear bending-torsion theory for inextensible rods by Gammaconvergence** *MiS Preprint Repository*

Mora MG, Müller S. (2004) **A nonlinear model for inextensible rods as a low energy Γ-limit of three-dimensional nonlinear elasticity** *Annales de l'Institut Henri Poincaré C* **21**:271–293

Moulton D, Lessinnes T, Goriely A. (2013) **Morphoelastic rods. Part I: A single growing elastic rod** *Journal of the Mechanics and Physics of Solids* **61**:398–427

Moulton DE, Lessinnes T, Goriely A. (2020) **Morphoelastic rods III: Differential growth and curvature generation in elastic filaments** *Journal of the Mechanics and Physics of Solids* **142**

Moulton DE, Oliveri H, Goriely A. (2020) **Multiscale integration of environmental stimuli in plant tropism produces complex behaviors** *Proceedings of the National Academy of Sciences* **117**:32226–32237

Nakajima K, Hauser H, Kang R, Guglielmino E, Caldwell DG, Pfeifer R. (2013) **A soft body as a reservoir: case studies in a dynamic model of octopus-inspired soft robotic arm** *Frontiers in computational neuroscience* **7**

Nardinocchi P, Teresi L. (2007) **On the active response of soft living tissues** *Journal of Elasticity* **88**:27–39

Norman KR, Moerman DG (2002) **α spectrin is essential for morphogenesis and body wall muscle formation in Caenorhabditis elegans** *The Journal of cell biology* **157**:665–677

Olson MF, Sahai E. (2009) **The actin cytoskeleton in cancer cell motility** *Clinical & experimental metastasis* **26**:273–287

Page AP, Johnstone I. (2007) **The cuticle** *WormBook*

Palumbo S, Benvenuti E, Fraldi M. (2022) **Actomyosin contractility and buckling of microtubules in nucleation, growth and disassembling of focal adhesions** *Biomechanics and Modeling in Mechanobiology* **21**:1–14

Priess JR, Hirsh DI (1986) **Caenorhabditis elegans morphogenesis: the role of the cytoskeleton in elongation of the embryo** *Developmental biology* **117**:156–173

Rodriguez EK, Hoger A, McCulloch AD (1994) **Stress-dependent finite growth in soft elastic tissues** *Journal of biomechanics* **27**:455–467

Saxena A, Denholm B, Bunt S, Bischoff M, VijayRaghavan K, Skaer H. (2014) **Epidermal growth factor signalling controls myosin II planar polarity to orchestrate convergent extension movements during Drosophila tubulogenesis** *PLoS biology* **12**

Schulz A, Dimitriyev M, Singal K, Sordilla S, Sahin A, Boyle C, Higgins C, Matsumoto E, Hu D. (2022) **Creating bio-inspired tissue mimics of African elephant trunks' wrinkled and folded skin** *APS March Meeting Abstracts* **2022**:Z08–10

Schulz AK, Boyle M, Boyle C, Sordilla S, Rincon C, Hooper S, Aubuchon C, Reidenberg JS, Higgins C, Hu DL (2022) **Skin wrinkles and folds enable asymmetric stretch in the elephant trunk** *Proceedings of the National Academy of Sciences* **119**

Serra M, Nájera GS, Chuai M, Spandan V, Weijer CJ, Mahadevan L. (2021) **A mechanochemical model recapitulates distinct vertebrate gastrulation modes** *bioRxiv* :2021–10

Shindo A, Wallingford JB (2014) **PCP and septins compartmentalize cortical actomyosin to direct collective cell movement** *Science* **343**:649–652

Shyer AE, Tallinen T, Nerurkar NL, Wei Z, Gil ES, Kaplan DL, Tabin CJ, Mahadevan L. (2013) **Villification: how the gut gets its villi** *Science* **342**:212–218

Soesanto T, Williams MC (1981) **Volumetric interpretation of viscosity for concentrated and dilute sugar solutions** *The journal of physical chemistry* **85**:3338–3341

Sulston JE, Schierenberg E, White JG, Thomson JN (1983) **The embryonic cell lineage of the nematode Caenorhabditis elegans** *Developmental biology* **100**:64–119

Tallinen T, Chung JY, Rousseau F, Girard N, Lefèvre J, Mahadevan L. (2016) **On the growth and form of cortical convolutions** *Nature Physics* **12**:588–593

Tan T, De Vita R. (2015) **A structural constitutive model for smooth muscle contraction in biological tissues** *International Journal of Non-Linear Mechanics* **75**:46–53

Telis VRN, Telis-Romero J, Mazzotti H, Gabas AL (2007) **Viscosity of aqueous carbohydrate solutions at different temperatures and concentrations** *International Journal of food properties* **10**:185–195

Toro R, Burnod Y. (2005) **A morphogenetic model for the development of cortical convolutions** *Cerebral cortex* **15**:1900–1913

Vicente-Manzanares M, Ma X, Adelstein RS, Horwitz AR (2009) **Non-muscle myosin II takes centre stage in cell adhesion and migration** *Nature reviews Molecular cell biology* **10**:778–790

Vuong-Brender TTK, Ben Amar M, Pontabry J, Labouesse M. (2017) **The interplay of stiffness and force anisotropies drives embryo elongation** *Elife* **6**

Vuong-Brender TTK, Suman SK, Labouesse M. (2017) **The apical ECM preserves embryonic integrity and distributes mechanical stress during morphogenesis** *Development* **144**:4336–4349

Williams BD, Waterston RH (1994) **Genes critical for muscle development and function in Caenorhabditis elegans identified through lethal mutations** *The Journal of cell biology* **124**:475–490

Yang X. (2017) **Yang X. Remodelage des jonctions sous stress mécanique. PhD thesis Université de Strasbourg; 2017.**

Yang Xinyi FT, Kelly Molnar NM, Loic Royer JP, Stephan Grill GM, Labouesse M. (2023) **Planar asymmetry in epithelial junction elongation results from repeated muscle contraction events** *Preprint Sorbonne University*

Zhang H, Landmann F, Zahreddine H, Rodriguez D, Koch M, Labouesse M. (2011) **A tension-induced mechanotransduction pathway promotes epithelial morphogenesis** *Nature* **471**:99–103

Zhukoski NE (1887) **Conference** *Comm Math Soc Kharkov* **17**:31–46

Article and author information

Anna Dai
Laboratoire de Physique de l'Ecole normale supérieure, ENS, Université PSL, CNRS, Sorbonne Université, Université Paris Cité, F-75005 Paris, France
ORCID iD: 0000-0002-5655-8885

Martine Ben Amar
Laboratoire de Physique de l'Ecole normale supérieure, ENS, Université PSL, CNRS, Sorbonne Université, Université Paris Cité, F-75005 Paris, France
For correspondence: martine.benamar@phys.ens.fr

Editors

Reviewing Editor
Claude Desplan
New York University, New York, United States of America

Senior Editor
Claude Desplan
New York University, New York, United States of America

Reviewer #1 (Public Review):

The authors have made a novel and important effort to distinguish and include different sources of active deformations for fitting C elegans embryo development: cyclic muscle contractions and actomyosion circumferential stresses. The combination and synchronisation of both contributions are, according to the model, responsible for different elongation rates, and can induce bending and torsion deformations, which are a priori not expected from purely contractile forces. The model can be applied to other growth processes in initially cylindrical shapes.

The tilt of the fibers is an important assumption of the model. However, fiber direction in Figure 3B is not fully clear for explaining the tilting. The fiber in 3B has not very much in common with the fibers in the color part of the figure. Also, is vector m supposed to be tangent to the fiber? In the figure does not seem to be so. It should be expected that alpha is a consequence of the deformation, not as an input parameter, as it seems in the tests of Figure 6A. How is the value of alpha chosen? According to Figure 6, torsion is expected for alpha>0, but for beta=pi/2 and alpha>0 no torsion may be obtained. In fact, it seems that torsion should appear when cos(beta)*sin(alpha)>0. As a consequence, value of beta should be given in Figure 6. Can the amount of torsion be tested as a function of alpha and beta?

The transfer of energy and deformation is a very interesting aspect of the paper, and also crucial for the model and predicting elongation. However, the modelling of this transfer remains very obscure and only explained in the Appendix. Some more details on how the transfer is selected should be given in the main text. Can the transfer of energy interpreted as a change of the relaxed reference configuration? Once a ratio of the energy transferred is fixed, the assumption on elongation distribution should be stated. (Uniformly?) The authors should also define in the main text the factor g_a1, and explain how this value is computed from condition W_c=W_r .

Given the convoluted shape of the embryo in the egg, contact may be a crucial mechanism for determining growth and torsion. The model does not include this contact, and this limitation should be reflected in the article.

Minor comment:
-Line 300: "we determine the optimal values for the activation parameters". the optimal with

respect to which objective? Norm of difference between experimental and computational displacements? How this is quantified needs to be specified.

https://doi.org/10.7554/eLife.90505.2.sa1

Reviewer #2 (Public Review):

Summary:

During C. elegans development, embryos undergo elongation of their body axis in absence of cell proliferation or growth. This process relies in an essential way on periodic contractions of two pairs muscles that extend along the embryo's main axis. How contraction can lead to extension along the same direction is unknown.

To address this question, the authors use a continuum description of a multicomponent elastic solid. The various components are the interior of the animal, the muscles, and the epidermis. The different components form separate compartments and are described as hyperelastic solids with different shear moduli. For simplicity, a cylindrical geometry is adopted. The authors consider first the early elongation phase, which is driven by contraction of the epidermis, and then late elongation, where contraction of the muscles injects elastic energy into the system, which is then transferred into elongation. The authors get elongation that can be successfully fitted to the elongation dynamics of wild type worms and two mutant strains.

Strengths:

The work proposes a physical mechanism underlying a puzzling biological phenomenon. The framework developed by the authors could be used to explain phenomena in other organisms and could be exploited in the design of soft robots.

Weaknesses:

(1) The manuscript is hard to read without being very familiar with continuum descriptions of elastic media. This might make the work difficult to access for biologists. This is a real pity because the findings are potentially of great interest to developmental biologists and engineers alike.

(2) The discussion of the worm's mechanical properties could go deeper. The authors hardly justify their assumptions.

https://doi.org/10.7554/eLife.90505.2.sa0

Author response:

The following is the authors' response to the original reviews.

> ***Recommendations for the authors:***
>
> ***Reviewer #1 (Recommendations For The Authors):***
>
> - *Line 144, after eq. (1). Vectors d_i need to be defined. Are these the mapping of vectors e_i due to the active deformation? It would be useful to state then that d_3 is aligned with r'.*

Thank you for your suggestion, and the definition has been added to lines 146-149 for a better understanding of the model.

> - *Line 144.Authors state a_i(0,0,Z)=0. Shouldn't this be true also for any angle, i.e., a_i(0,Theta, Z)=0?*

Thank you, we have revised it in line 144.

> - *Line 156. G_0 is defined as Diag(1,g_0(t), 1), which seems to be using cylindrical coordinates. Previously, in line 147, vector argument X of \chi is defined with Cartesian coordinates (X,Y,Z). Shouldn't these be also cylindrical?*

We are very sorry for this error, our initial configuration is defined with cylindrical coordinates, we have revised it in the manuscript line 151.

> - *Line 162. "where alpha and beta lie in the range [-pi/2, pi/2]" has already been indicated.*

Thank you for your mention, we have deleted duplicate information in line 166.

> - *Line 171. W is defined as the strain energy density, while in equation (2), symbol W is the total energy (which depends on the previous W). Letters for total elastic and strain energy must be distinguished.*

Thank you, we have changed the letter for total energy in Eq.(2).

> - *Line 176. "we take advantage of the weakness of" -> "we take advantage of the small value of".*

We have revised it in line 179.

> - *Line 177. Why is there a subscript i in p_i? If these do not correspond to penalty p, but to parameters in eqn (3), the latter should have been introduced before this line.*

We have revised this error in line 180.

> - *Line 186. "as the overall elongation \zeta". This parameter, axial extension, has not been defined yet.*

Thank you for your mention, the definition of \zeta is now given in line 146.

> - *Figure 4. Why are the values of g_0 from the elastic model and equations (30)-(32) so non-smooth? Clarify what is being fit and what is the input in the latter equations. Final external radius R_3? Final internal radius R_1'?*

(1) To mimic the embryo, we consider a multi-layered cylindrical body so that the shear modulus of each layer is different. The continuity of both deformations and stresses is imposed (see Eq.(26)-Eq.(30). This is the usual treatment for complex morpho-elastic systems. Obviously, g_0 originates from the actomyosin cortex so it appears only in the

corresponding layer. Finally, all physical quantities such as deformations and stresses must be continuous.

(2) The final outer radius is R_3, which represents the outer radius of C. elegans embryos. In addition to R_3, what we need to consider in this model are R_1'=0.7, R_1'=0.768, R_2=0.8 and R_2'=0.96, these definitions have been added in the caption of Appendix 2—figure 1.

> - *Line 663, equation (19). Parameter mu is multiplying penalisation term with p, while in equation (2) mu is only affecting the elastic part.*

These two different ways of expressing the energy function will ultimately affect the value of p, but the two p are not the same quantities, so they will not affect our results. To avoid misunderstandings, we will replace p in equation (19) with q.

> ***Reviewer #2 (Recommendations For The Authors):***
>
> *As mentioned in my public summary, I find the writing really not adequate. I provide here a list of specific points that the authors should in my opinion address. As a general comment, I would delete many instances of 'the'.*
>
> *First, here are figures and whole paragraphs that do not seem to bring anything to the understanding of the phenomenon of C. elegans elongation, notably, Figs. 2, 3C-H, 5m, and 6. Figures 6G and 7 are the only figures containing results it seems. Some elements of the figures are repeated, for example, the illustration of the system's cross-section in Figs 3 and 5.*

Thank you for your suggestion, we have made some adjustments to our images to remove some of the duplicate information.

> *Second, and this is my most important criticism: the mechanism of elongation by releasing elastic stress introduced by muscle contraction is not explained in clear terms anywhere in the text. At least, I was unable to understand it. On p 10 you write "This energy exchange causes the torsion-bending energy to convert into elongation energy, (...)" How this is done is not explained. I assume that the reference state is somehow changed through muscle contraction. The new reference state probably has a longer axis than the one before, but this would then be a plastic deformation and not purely elastic as claimed by the authors (ll 76: "This work aims to answer this paradox within the framework of finite elasticity without invoking cell plasticity (...)"). Is torsion important for this process or is it 'just' another way to store elastic energy in the system?*

We perfectly explain most of the exchange of energy between bending, torsion and elongation: indeed, we quantify all aspects of this transformation as the elastic elongation energy, and the dissipation processes which will cost energy. The dissipation evaluated here concerns the rotation of the worm due to the muscle geometry and the viscous friction at the inner surface of the egg. Torsion seems to appear in the late stages and only in some cases. As we show, it comes from a torque induced by the muscles which are not vertical. vertical. Finally, our quantitative predictions of the modelling which recovers most of the experimental published results.

> *Third, there are a number of strange phrasings and the notation is not helpful in places.*

We feel sorry for that, the manuscript is now more precise.

> *Fourth, the title promises to explain how cyclic muscle contractions reinforce acto-myosin motors. I can't see this done in this work.*

The fact that the acto-myosin is reorganized between two sequences of contraction justifies the title. The complete reorganization of the actomyosin network would require a chemico-mechanical model that is not achieved here, perhaps in future work as data become available.

> *In addition:*

We have chosen to respond globally rather than point by point to the referee's recommendations.

> *Typographic errors and vocabulary*

All English corrections and typos are now included in the main text.

> *Figures and captions:*

Figures and captions have been improved.

> - *Figure 1: Make the caption and the illustration more coherent. For example, only two cell types are distinguished; in the caption, you mention lateral cells, in the sketch seam cells. What is the difference between acto-myosin and muscle contraction? Muscle contraction is also auto-myosin-based.*

(1) The caption for Fig.1 is revised.

(2) From a mechanical point of view, actomyosin bundles in C elegans are orthoradial, whereas muscles are essentially parallel to the main axis of the body are essentially parallel to the main axis of the body, so the geometry is completely different and of extreme importance for deformation. Muscle contractions are quasi-periodic, we do not know the dynamics of the attached molecular motor of myosin. So of course, both contain actin and myosin (not exactly the same proteins), but our model is sensitive to more macroscopic properties.

> - *Figure 2: I do not find this figure helpful. I might expect such a figure in a grant proposal, but much less in an article.*

Figure 2 shows the strategy of our work, we hope that readers can see at a glance what kind of analysis has been done through this figure: since our work is divided into several parts, readers can also unravel the logic through this scheme after reading the whole manuscript. So, this diagram is a guide, and it may be helpful and necessary.

> - *Figure 3: Figure 3 A, right: What is the dashed line? B You indicate fibers, but your model does not contain fibers, does it? How do I get from the cube to the deformed object? What is the relation of C-H with the rest of the work? Furthermore, you mention seam cells in Fig. 1, but they are absent here. Why can you neglect them? Why introduce them in the first place? E What is a plant vine? F-H What rods are you referring to? Plants do not have muscles, right?*

We have modified this figure, and the original Figure 3 now corresponds to Figures 3 and 4.

(1) The dashed line is the centerline after deformation.

(2) The referee is wrong: our model represents the fibers by a higher shear modulus for the actomyosin cortex and for the muscles (see Table Appendix 1) and G_1 reflects the activities of the muscle and actin fibers.

(3) The cube in Figure 3 is a mathematical 3D volume element that is subjected to stresses. Hyperelasticity modelling is based on such a representation.

(4) C-H(new version: Fig.4 A-F): These images show similar deformations: bending and torsion as our C. elegans study. These figures indicate that such deformations are quite common in nature, even if the underlying mechanism is different.

(5) This is a point we have already mentioned: we ignore the difference between the different types of epidermal cells and average their role in the early and second stages of elongation.

(6) The plant vine is the 'botanical vine', see Goriely's article and book.

(7) F-H(new version: Fig.4 D-F) do not have fixed rods, we set a curvature and torsion to fit the actual biological behavior.

(8) Plants do not have muscles, but they grow, and our formalism for growth, pre-strain and material plasticity is very similar to the hyper-elasticity formalism.

- *Figure 4: Fig .4 A: "The central or inner part ($0 < R < R2$, shear modulus μ_1) except the muscles which are stiffer." I do not understand.*

In the new version, this figure corresponds to Fig.5. The shear modulus of the intrinsic part is very small, but the muscles are harder so we have to consider them separately, we have revised this sentence to avoid misunderstanding.

- *Figure 5: Fig 5 A and D: The schematic of the cross-section has appeared already in the previous figure. No need to repeat it here. The same holds for the schematic of the cylindrical embryo. Caption: "But, the yellow region is not an actual tissue layer and it is simply to define the position of muscles." Why do you introduce the yellow region at all? I do not think that it clarifies anything. "Deformation diagram, when left side muscles M_1 and M_2." Something seems to be missing here. Similarly in the next sentence. "the actin fiber orientation changes from the 'loop' to the 'slope'" Do the rings break up and form a helix?*

In the new version, this figure corresponds to Fig.6.

(1) We have made revisions to these figures.

(2) The yellow part can show the accurate location of four muscles, which is important for our model and further calculations.

(3) We have revised this sentence in the caption of Fig. 6.

(4) Actin rings do not change to a helix pattern, they will be only sloping.

- *Figure 6: Fig 6 A-C These panels do not go beyond Fig 5B. Fig 6D: what are these images supposed to show? They are not really graphs, but microscopy images. The caption is not helpful to understand, what the reader is supposed to see here. Fig 6F: do you really want to plot a linear curve?*

In the new version, Fig.5 and Fig.6 respectively correspond to Fig.6 and Fig.7.

(1) Fig.6 shows the simulated images, and Fig.7 A-C is the real calculation results, they are different.

(2) Fig.7 D can show the real condition during C. elegans late elongation, here, we would like to show the torsion of the C. elegans.

(3) Yes, it is our result.

> *Discussions concerning the biological referee questions:*
>
> *Ll 75: “how the muscle contractions couple to the acto-myosin activity" Again I find this misleading because muscle contraction relies on auto-myosin activity. Probably, you can find a better expression to refer to the activity of the actomyosin network in the epidermis. Do you propose any mechanism for how muscle contraction increases epidermal contractility? This does not seem to be the mechanism that you propose for elongation, is it?*

The actomyosin activity will not stop because of the muscle contraction. Obviously, these two processes cannot be independent. The energy released by a muscle contraction event can and must contribute to the reorganization of the actomyosin network that occurs during the elongation process. Indeed, despite the fact that the embryo elongates, the density of actin cables appears to be maintained, which automatically requires a redistribution of actin monomers. We propose a scenario in which muscle contraction increases actomyosin contractility via energy conversion. We show that after unilateral contraction there is an energy release for this once all dissipation factors are eliminated. We invite the reviewer to re-examine Figure 2 and invite biologists to seriously evaluate the density of molecular motors attached to the circumferential actin cable throughout the stretch process.

> *Ll 133: "we decide to simplify the geometrical aspect because of the mechanical complexity" This is hardly a justification. Why is it appropriate?*

Yes, we would like to offer the reader the simplest modelling with a limiting technicity and a limited number of unknown parameters.

> *L 135: "active strains" Why not active stress?*

The two are equivalent, the choice is dictated by the simplicity of deriving quantitative results for comparison with experiments.

> *L 170: "hyperelastic" Please, explain this term.*

It is the elasticity of very soft samples subjected to large deformations. For classic references, see the books of Ogden, Holzapfel and Goriely, all of which are mentioned in our paper.

> *Major criticism*
>
> *Eq. 3 and Ll 227: "p_1 is the ratio between the free available myosin population and the attached ones divided by the time of recruitment" Why is the time of recruitment the same for all motors? "inverse of the debonding time" Is it the same as the unbinding rate? Why use the symbol p_2 for it? What is p_3?*

The model proposed to justify the increase in the activity of the actomyosin motors during the first phase is a mean-field model: thus all quantities are averaged: we are not considering the theory of a single molecular motor, but a collection in a dynamic environment, so we do not need stochasticity here. Equation (3) concerns the compressive pre-strain, which by

definition is a quantity varying between 0 and 1 and $X_g=1-G$. ... The debonding time is not the same as the debonding rate. The term p_3 indicates saturation and is derived from the law of mass action. The good agreement with the experimental data is shown in Fig.5 (A) and (B). An equivalent model has been developed by (M. Serra et al.).

Serra M, Serrano Nájera G, Chuai M, et al. A mechanochemical model recapitulates distinct vertebrate gastrulation modes[J]. Science Advances, 2023, 9(49)

> *Ll 275: "This energy exchange causes the torsion-bending energy to convert into elongation energy, leading to a length increase during the relaxation phase, as shown in Fig.1 of Appendix 5." You have posed the puzzle of how contraction leads to elongation, and now that you resolve the puzzle, you simply say that torsion and bending energy are converted into elongation. How? Usually, if I deform an elastic object, it will return to its original configuration after releasing the external forces. Why is this not the case here?*
>
> *Furthermore, the central result of your work is presented in an Appendix!?*

We agree with the referee that an elastic object will return to its initial configuration by releasing stress, i.e. by giving up its accumulated elastic energy to the environment. But the elastic energy has to go somewhere, such as heat. We do not dare to say that the temperature of the worm increases during the muscle contractions.

In fact, the referee's comment also assumes that full relaxation of the stresses is possible, so the object is not a multi-layered specimen and/or it is not enclosed in a box. Most living species are under stress, usually called residual stress. Our skin is under stress. Our fingerprints result from an elastic instability of the epidermis, occurring on foetal life as our brain circumvolutions or our vili. . So, it is obvious that stresses are maintained in multilayered living systems. Closer to the case of C. elegans, the existence of stresses has been demonstrated by experiments with laser ablation fractures in the first stage. The fact that the fractures open proves the existence of stress: if not, there is no opening and only a straight line.

> *Ll 379: "Although a special focus is made on late elongation, its quantitative treatment cannot avoid the influence of the first stage of elongation due to the acto-myosin network, which is responsible for a prestrain of the embryo." This statement is made repeatedly through the manuscript, but I do not understand, why you could not use an initial state without pre-strain.*

This is the basic concept of hyperelasticity. The reference state must be free of stress, so we cannot evaluate the first muscle contraction without treating the first elongation stage.

> *Grammar, vocabulary and writing errors*
>
> *ll 31: "the influence of mechanical stresses (...) becomes more complex to be identified and quantified" Is the influence of mechanical stress too complex or too difficult to be identified/quantified?*

We have revised it in line 31, “The superposition of mechanical stresses, cellular processes (e.g., division, migration), and tissue organization is often too complex to identify and quantify.”

> *Ll 41: "The embryonic elongation of C. elegans represents an attractive model of matter reorganization without a mass increase before hatching." Maybe "Embryonic elongation of C. elegans before hatching represents an attractive model of matter reorganization in the absence of growth.".*

We have revised it in line 41.

> *L 42: "It happens after the ventral enclosure (...)" Maybe "It happens after ventral enclosure (...)".*

We have revised it in line 42.

> *Ll 52: "The transition is well defined since the muscle participation makes the embryo rather motile impeding any physical experiments such as laser ablation (...)" Ablation of what?*

We have revised it in line 53:The transition is well defined, because the muscle involvement makes the embryo rather motile, and any physical experiments such as laser fracture ablation of the epidermis, which could be performed and achieved in the first period (\cite{vuong2017interplay}), become difficult,.

> *Ll 59: "a hollow cylinder composed of four parts (seam and dorso-ventral cells)" It is not clear, what the four parts are - in the parenthesis, two are mentioned.*

We have revised it in line 59. Fig.1 shows the whole structure, dorsal, ventral and seam cells form four parts of the epidermis.

> *L 78: "several important issues at this stage remain unsettled" At which stage?*

It means the late elongation stage, we have added this information in line 78.

> *Ll 85: "but how it works at small scales remains a challenge." Maybe "but how it works at small scales remains to be understood.".*

We have revised it in line 86.

> *Ll 99: "the osmolarity of the interstitial fluid" The comes out of the blue. Before you only talked about mechanics, why now osmolarity? Also, the interstitial fluid is only mentioned now. It is important for the dissipative effects that you discuss later, right? If yes, then you should probably introduce it earlier.*

For a better understanding, we have change osmolarity into viscosity in line 99.

> *l 120: "The cortex is composed of three distinct cells" Maybe "distinct cell types".*

Thank you, and we have revised it in line 120.

> *L 121: "cytoskeleton organization and actin network configurations" What is the difference between cytoskeleton organization and actin network configuration? Also, either both should be plural or both singular, I guess.*

(1) Cytoskeleton (which involves microtubules) forms the epidermis of C. elegans embryos, and the actin network surrounds the epidermis.

(2) Thank you for your suggestion, we have revised it in line 121.

> *L 130: "which will be introduced hereafter" Maybe "which will be used hereafter".*

We have revised it in line 130.

> *Ll 148: "The geometric deformation gradient" You usually denote vectors in bold face, so \chi should be bold, right? Define d_i in Eq.(1).*

Yes, we have added this information in line 147.

> *L 172: "auxiliary energy density" Please, explain this term.*

We have changed "auxiliary energy density" into "associated energy density" in line 175. Energy density is the amount of energy stored in a given system or region of space per unit volume, the associated energy density in our manuscript can help us to do some calculations.

> *Ll 188: "Similar active matter can be found in biological systems, from animals to plants as illustrated in Fig.3(C)-(E), they have a structure that generates internal stress/strain when growing or activity. (...)" Why such a general statement during the presentation of the results? The second part of the sentence seems to be incomplete.*

Answers: We would like to show our method is general, and can be used in many situations. We have revised the wrong sentence in line 192.

> *Ll 243: "a bending deformation occurs on the left for active muscles localized on left" Maybe "bending to the left occurs if muscles on the left are activated".*

Thank you, we have revised it in line 247.

> *L 250: "we assume them are perfectly synchronous" Maybe "we assume them to contract simultaneously". We have revised it in line 252.*
>
> *L 258: "the muscle and acto-myosin activities are assumed to work almost simultaneously." Before it was simultaneously, now only almost!? What does almost mean?*

Sorry, we would like to express the same meaning in theses two sentences, we have deleted the word ‘almost’ in line 261.

> *Ll 294: "one can hypothesize several scenarios" After that, only one scenario is described it seems.*

Thank you, we have revised this sentence in line 299.

> *L 341: "and then is more viscous than water" Maybe "and that is more viscous than water".*

We have revised it in line 345.

> *L 373: "before the egg hatch" Maybe "before the embryo (or larva) hatches"?*

We have revised the sentence in line 367.

> *L 409: "elephant trunk elongated" maybe "elephant trunk elongation".*

We have revised it in line 412.

> *Ll 417: "As one imagines, it is far from triviality (...)" Does this remake help in any way to understand better C. elegans elongation? Also maybe "it is far from trivial".*

We have revised it in line 423.

> *Ll 428: "can map the initial stress-free state B_0 to a state B_1, which reflects early elongation process" Maybe: "maps the initial stress-free state B_0 to a state B_1, which describes early elongation".*

We have revised it in line 428.

> *L 429: "After in the residually stressed (...)" Maybe "Subsequently, we impose an incremental strain filed G_1 that maps the state B_1 to the state B_2, which represents late elongation".*

We have revised it in line 429.

> *l 763: "Modelling details of without pre-strain case" Maybe "Case without pre-strain" or "Modelling in the absence of pre-strain" Similarly for l 784.*

We have revised them in line 763 and line 784.

> *Some questions of definition and understanding*
>
> *Ll 71: "We can imagine that once the muscle is activated on one side, it can only contract, and then the contraction forces will be transmitted to the epidermis on this side." I do not understand the sentence. Muscle activation leads to contraction, there is nothing to imagine here. Maybe you hypothesize that the muscles are attached to the epidermis such that muscle contraction leads to epidermis deformation?*

Yes, four muscle bands are attached to the epidermis, as shown in Fig.1. The deformation does not concern only the epidermis but the whole embryo during the bending events. We have modified the sentence to avoid misunderstanding, the sentence change to “Once the muscle is activated on one side, it can only contract, and then the contraction forces will be transmitted to the epidermis on this side.” in line 71.

> *Ll 110: "However, it is less widely known that its internal striated muscles share similarities with skeletal muscles found in vertebrates in terms of both function and structure" Is it important for what you report, whether this fact is widely known?*

Yes, it is our opinion.

> *Ll 112: "the role of the four axial muscles (...) is nearly contra-intuitive" Is it or is it not? If yes, why?*

Yes it is. Muscles exert contractions, so compressive deformations. Their localization are along the axis of symmetry (up to a small deviation) so they cannot mechanically realize the expected elongation, contrary to the orthoradial actomyosin network.

However, elongation of the C. elegans is observed experimentally, so yes, we think the result contraintuitive.

> *L 116: "fully heterogeneous cylinder" What is this?*

It means that the C. elegans embryo does not have the same elastic properties in different parts (or layers).

> *L 129: "will collaborate to facilitate further elongation" To facilitate or to drive? If the former, what drives elongation?*

Contraction of muscles and actin bundles together drive elongation

> *Ll 141: "the deformation in each section can be quantified since the circular geometry is lost with the contractions" The deformation could also be quantified if the sections remained circular, right?*

Yes. However, circularity is lost during each bending event.

> *Ll 151: "we need to evaluate the influence of the C. elegans actin network during the early elongation before studying the deformation at the late stage. So, the deformation gradient can be decomposed into: (...) where (...) is the muscle-actomyosin supplementary active strain in the late period" I thought you were now studying the early stage?*

In this part, we are outlining how we can study the whole elongation (early and late), not just the early elongation stage. To evaluate the deformation induced by the first contraction of the muscles, we need to know the state of stress of the worm prior to this event, so we also need to recover the early period using the same formalism for the same structure.

> *L 160: "When considering a filamentary structure with different fiber directions" Which filamentary structure are you talking about?*

Fig.3 B shows this model and the filamentary structure, which contains the actin and muscle fibers.

> *Ll 174: "When the cylinder involves several layers with different shear modulus μ and different active strains, the integral over $\mathcal{S}$ covers each layer" I do not understand this sentence. Also, you should probably write 'moduli' instead of modulus.*

This implies that when integrating over the whole cross-section S, we need to take into account each layer independently with its own shear modulus and sum the results.

> *L 176: "weakness of ε" Do you mean \epsilon << 1?*

Yes

> *Ll 178: "Given that the Euler-Lagrange equations and the boundary conditions are satisfied at each order, we can obtain solutions for the elastic strains at zero order $\boldsymbol{a(0)}$ and at first order $\boldsymbol{a(1)}$." Are you thinking about different orders in an \epsilon expansion or the early and the late stages of elongation?*

Answers: Different orders are considered only for the late elongation study, the early elongation is treated exactly so do not need a correction in \epsilon.

> *L 197: "fracture ablation" Please, define.*

This is an experiment in which a laser is used to make a cut in a small-scale object of study and then the internal stresses are obtained based on the morphology of the cut, please see the

Ref ‘Assessing the contribution of active and passive stresses in C. elegans elongation’. We have added this definition in line 200.

> *Ll 203: What motivated your choice of notations for the radii R_2'? The inner part of the cylinder is fluid? But above you wrote about a solid cylinder. Why should the inner part be compressible?*

(1) We need to define the location of actin cables, which concentrate at the outer periphery.

(2) Our model is a hollow cylinder, and the inner part of the cylinder contains internal organs, tissues, fluids, and so on, so we consider it to be a compressible extremely soft material (Line 213).

> *Ll 212: "$r(R)$ is the radius after early elongation." And during?*

R is variable, r(R) depends on R but also on time t, it represents the radius of C. elegans embryos after the onset of elongation, i.e., after acto-myosin and muscle activities begin.

> *L 232: \tau_p is probably t_p?*

Yes.

> *L 240: "quite simultaneously" Please, be precise.*

In practice, it is difficult to define the concept of simultaneous occurrence unless there is rigorous experimental data to show it, but all we can get in the Ref ‘Remodelage des jonctions sous stress mécanique’, is that it occurs almost simultaneously, which we define as quite simultaneously.

> *Ll 246: "a short period" What does short mean? Why is it relevant?*

From the experimental observations and data, we know that each contraction occurs very rapidly: a few seconds so we define a short period for one contraction.

> *L 263: "the bending of the model will be increased" Is it really the model that is bent?*

Yes, the bending deformation predicted by the model, we have revised in line 266.

> *Ll 265: "we observed a consistent torsional deformation (Fig.6(E)) that agrees with the patterns seen in the video" In which sense do these configurations agree? I do not see any similarity between panels D and E.*

Both show a torsion deformation.

> *L 267: "torsion as the default of symmetry of the muscle axis" I do not understand.*

We discuss two cases in this research, one where the muscle follows the axis of the C. elegans in the initial configuration, and the other where the muscle has a slight angle of deflection, and we have added more information in the manuscript (line 270).

> *Ll 274: "Each contraction of a pair increases the energy of the system under investigation, which is then rapidly released to the body." Do you mean the elastic energy stored in the epidermis and central part of the embryo?*

Yes, the whole body.

> *Ll 284: "The activation of actin fibers g_{a1} after muscle relaxation can be calculated and determined by our model." Have you done it?*

Yes, we can obtain the value of g_a1, and then calculate the elongation.

> *Ll 286 I do not understand, why you write about mutants at this place. Am I supposed to have already understood the basic mechanism of elongation? Why do you now write about the first stage?*

I would like to show our formalism can model wild-type and mutant C.elegans, and the comparison results are good.

> *L 302: "The result is significantly higher than our actual size 210μm." How was significance assessed? Your actual size is probably more than 210μm.*

Here, we have considered two situations, one is that the accumulated energy is totally applied to the elongation so that the length will be much larger than the experimental result of 210 μm, the length value that we have obtained by calculation. In the other case, we have considered the energy dissipation, which leads to 210 μm.

> *L 433: "where λ is the axial extension due to the pre-strained" Maybe ""where λ is the axial extension due to the pre-stress".*

In our manuscript, we define the pre-strain, not the pre-stress.

> *L 438: "active filamentary tensor" Please, define.*

Active filamentary tensor defines the tensor representing the activities of a cylindrical model composed of different orientations fibers.